AD NUMBER

AD218493

NEW LIMITATION CHANGE

TO

Approved for public release, distribution unlimited

FROM

Distribution authorized to U.S. Gov't. agencies and their contractors; Administrative/Operational Use; JAN 1958. Other requests shall be referred to Office of Naval Research, 800 North Quincy Street, Arlington, VA 22217-5660.

AUTHORITY

ONR ltr, 26 Oct 1977

SECURITY INFORMATION
Unclassified

[redacted]

REPORT NUMBER
F-58-1

[redacted]

PURDUE UNIVERSITY
ROCKET LABORATORY

LAFAYETTE, INDIANA

EXPERIMENTAL DETERMINATION OF THE HEAT FLUX DISTRIBUTION IN A ROCKET NOZZLE

Robert Koeberle Rose

Contract N7 onr 39418

SECURITY INFORMATION
Unclassified

ISSUE DATE
January 1958

PURDUE UNIVERSITY

and

Purdue Research Foundation

Lafayette, Indiana

Report No. F-58-1

EXPERIMENTAL DETERMINATION OF THE HEAT FLUX DISTRIBUTION IN A ROCKET NOZZLE

Robert Koeberle Rose

Final Report 58-1

Contract N7 onr 39418

Rocket Laboratory

January 1958

ACKNOWLEDGMENTS

The author wishes to express his gratitude to his major professor Dr. M. J. Zucrow for his counsel during the course of this research program and to Dr. C. F. Warner for his technical advice and assistance. The author also thanks Dr. B. A. Reese for his valuable suggestions on the preparation of this thesis.

Special credit is given to Mr. Wayne H. Munyon, Undergraduate Technician, for his personal interest and invaluable assistance. Recognition is given to Mr. C. D. Merkel who constructed the nozzle which was employed during the investigation and to Mr. V. D. Hendricks, Instrument Technician. The author is also indebted to Mr. D. L. Crabtree for the preparation of the figures and reduction of data presented in this report, and to Mrs. Helen Booth and Mrs. Jean Patterson for the typing of the manuscript.

This work was sponsored by the Office of Naval Research under Contract N7 onr-39418 and their assistance and interest is gratefully acknowledged. Reproduction in full or in part is permitted for any use of the United States Government.

TABLE OF CONTENTS

TABLE OF CONTENTS (Continued)

LIST OF TABLES

LIST OF ILLUSTRATIONS

LIST OF ILLUSTRATIONS (Continued)

ABSTRACT

This report presents experimental values of the heat flux distribution in the exhaust nozzle of a rocket motor burning WFNA-NH_3 propellants at combustion pressures of 500 and 600 psia over the mixture ratio range 1.4 to 3.0. In addition, two runs were made at an increased combustion pressure of approximately 1000 psia. Local gas film coefficients and wall temperatures were calculated at each section of the nozzle for all data points, and the local Nusselt number was correlated in terms of the Reynolds and Prandtl numbers.

Values of the wall temperature and heat flux distribution calculated by the afore-mentioned correlation equation, by the methods of Bartz and of Sibulkin are compared with the experimental values.

The data for calculating the performance parameters for the rocket motor were measured during each of the runs for determining the heat transfer rates.

INTRODUCTION

The object of the investigation reported herein was to determine the axial variation of heat flux for a rocket nozzle and to compare the experimental values with those calculated by employing equations presented in the literature (1)(2)(21).* A correlation equation for the local gas film coefficient was also obtained from measurements of the local heat flux.

To obtain experimental values of the local heat flux in a rocket nozzle, static rocket motor firings were conducted at the Purdue University Rocket Laboratory employing a nominal** 200 lb thrust rocket motor burning the propellants WFNA (white fuming nitric acid) and liquid ammonia. A specially designed nozzle was utilized which made it possible to obtain six measurements of the local heat flux.***

---

* Numbers in parentheses refer to Bibliography.

** Although at the higher chamber pressures the rocket motor developed more than 200 lbs thrust, the initial design conditions specified 200 lbs thrust at a chamber pressure of 500 psia.

*** The complete calculations, and all of the data are presented in Reference 27.

DESCRIPTION OF APPARATUS

Rocket Motor Components and Control System

For the purpose of measuring the heat flux distribution in the nozzle of a rocket motor, a rocket motor was designed to operate at 500 psia combustion pressure and 200 lbs thrust with a propellant combination of WFNA (white fuming nitric acid) and liquid ammonia. The characteristic length, L*, of the motor was 80 inches. The rocket motor test stand with its associated control, instrumentation and feed lines is shown in Fig. 1. The experimental nozzle is located in the left center of the figure. The rocket motor was operated from the main control panel shown in Fig. 2. The pressure regulators and pressure gages associated with the propellant tanks and purge system are mounted on the upper right hand panel.

Hydraulic Throttling Valves

Two hydraulic throttling valves which could be controlled from the lower right hand panel were employed to vary the propellant flow rates. As the start was always made at stoichiometric mixture ratio, the mixture ratio was either from stoichiometric to high or stoichiometric to low mixture ratio. A by-pass arrangement was incorporated in the valves which allowed approximately 70 per cent of full flow when the valves were completely closed. This by-pass arrangement made it possible to obtain the correct startup flow rates by setting the propellant tank pressures. After the start was initiated, the control valves were regulated until the fuel and oxidizer flow rates corresponded to previously determined run points.

The fire switch and actuating switches for pressurizing, purging,

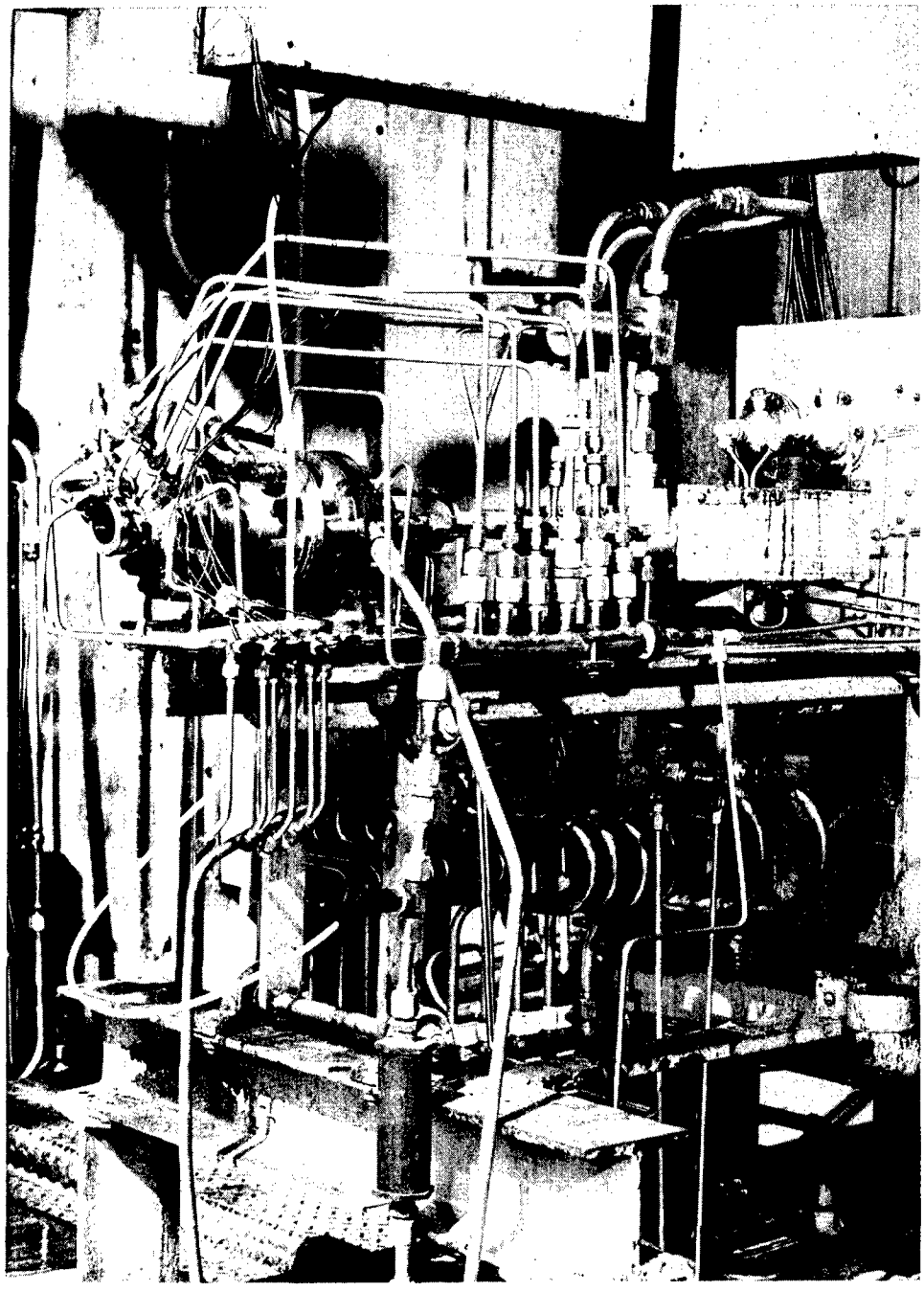

Fig. 1, Rocket Motor Test Stand

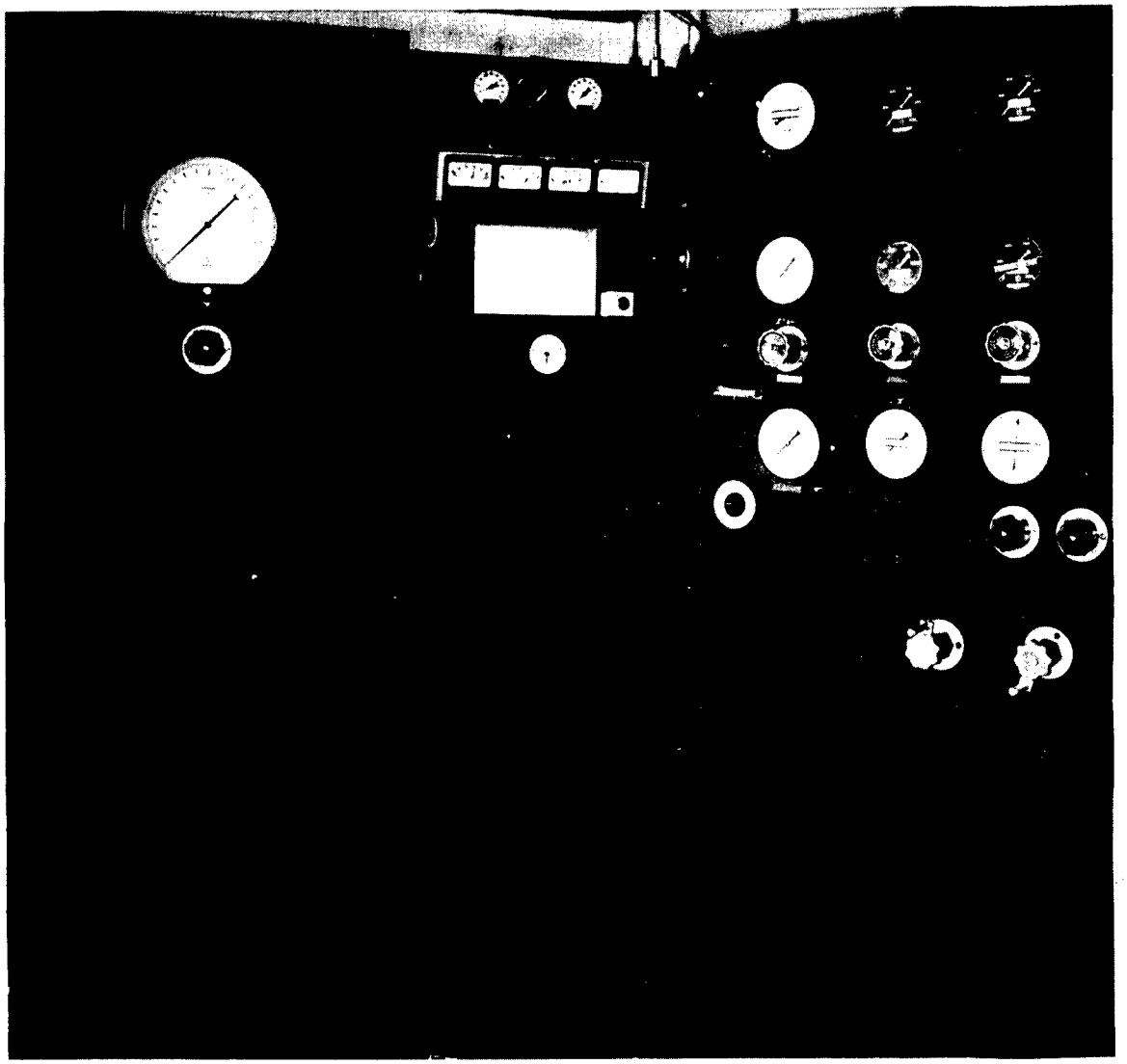

Fig. 2 Main Control Panel

and venting are located on the central panel.

Sectional Nozzles

Two sectional nozzles were employed during the investigation reported herein. Figure 3 is an assembly drawing of the first nozzle. The nozzle was made up of twelve sections which were aligned with two 1/2 in dowel pins and bolted together. To prevent gas leakage to the atmosphere, an O-ring seal was employed between sections, and, as an added precaution, a graphite-water emulsion was painted on each section prior to assembly. This method of sealing worked satisfactorily and no gas leakage occurred.

Each of the 12 sections was composed of two parts, an inner coolant channel which was exposed to the hot combustion gas and an outer retaining ring into which the coolant channel was welded. Two radial inlet and outlet holes were drilled in the retaining ring to provide each coolant passage with an independent coolant supply.

Figure 4 is a photograph of a partial assembly of the nozzle with the indexing pins in place.

When the first run was made using the afore-mentioned nozzle it was noted on shutdown that all of the coolant passages were leaking at the welds. The coolant passages were pressure tested to 1000 psi prior to the first run, and thus the leaks must have developed either during the run or at shutdown (when the full coolant pressure was across the hot walls of the inner coolant channel). An attempt to repair the nozzle by rewelding the sections was unsuccessful because the sections warped when they were welded and there was no excess metal on the sections to permit finish machining.

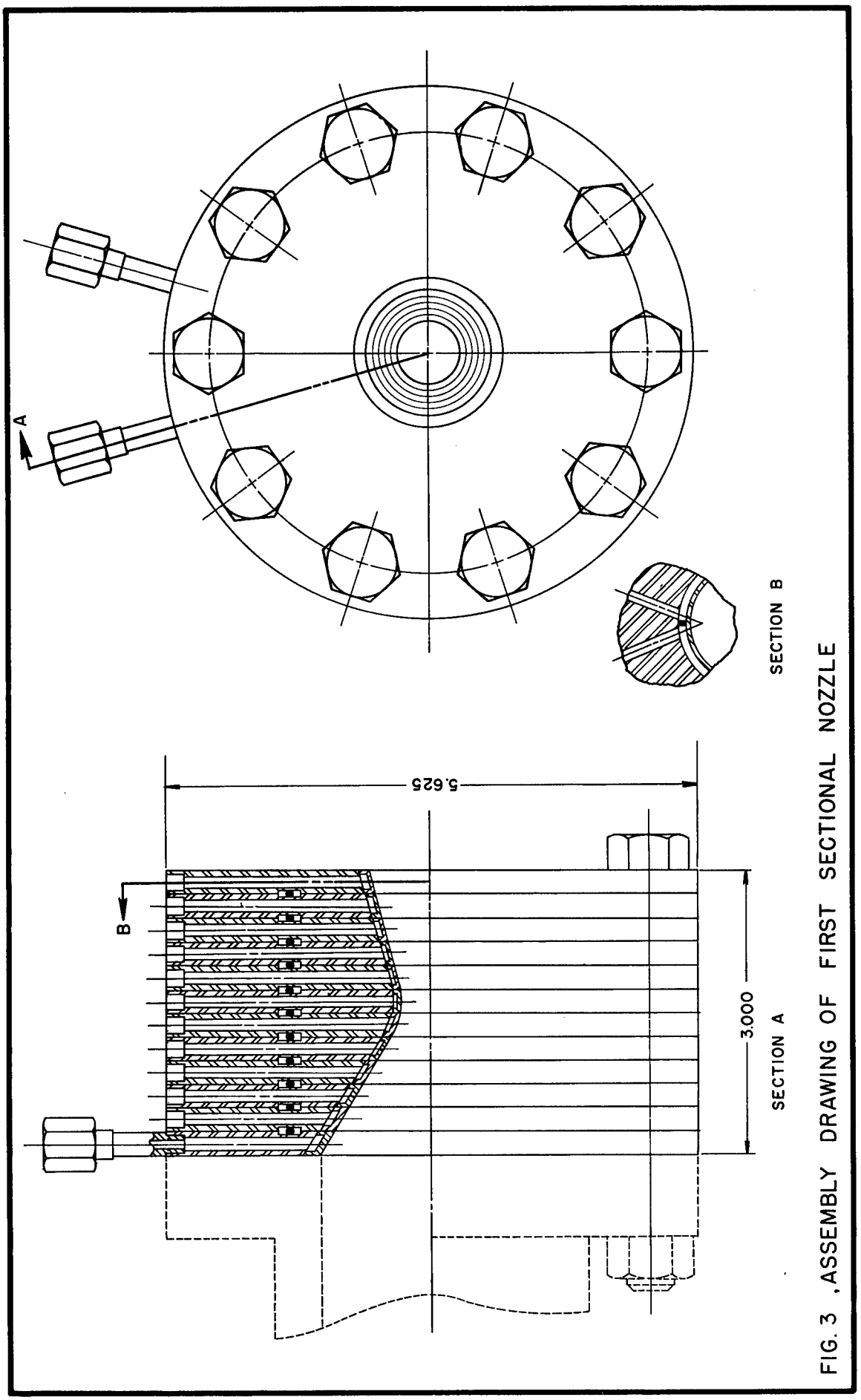

FIG. 3 ,ASSEMBLY DRAWING OF FIRST SECTIONAL NOZZLE

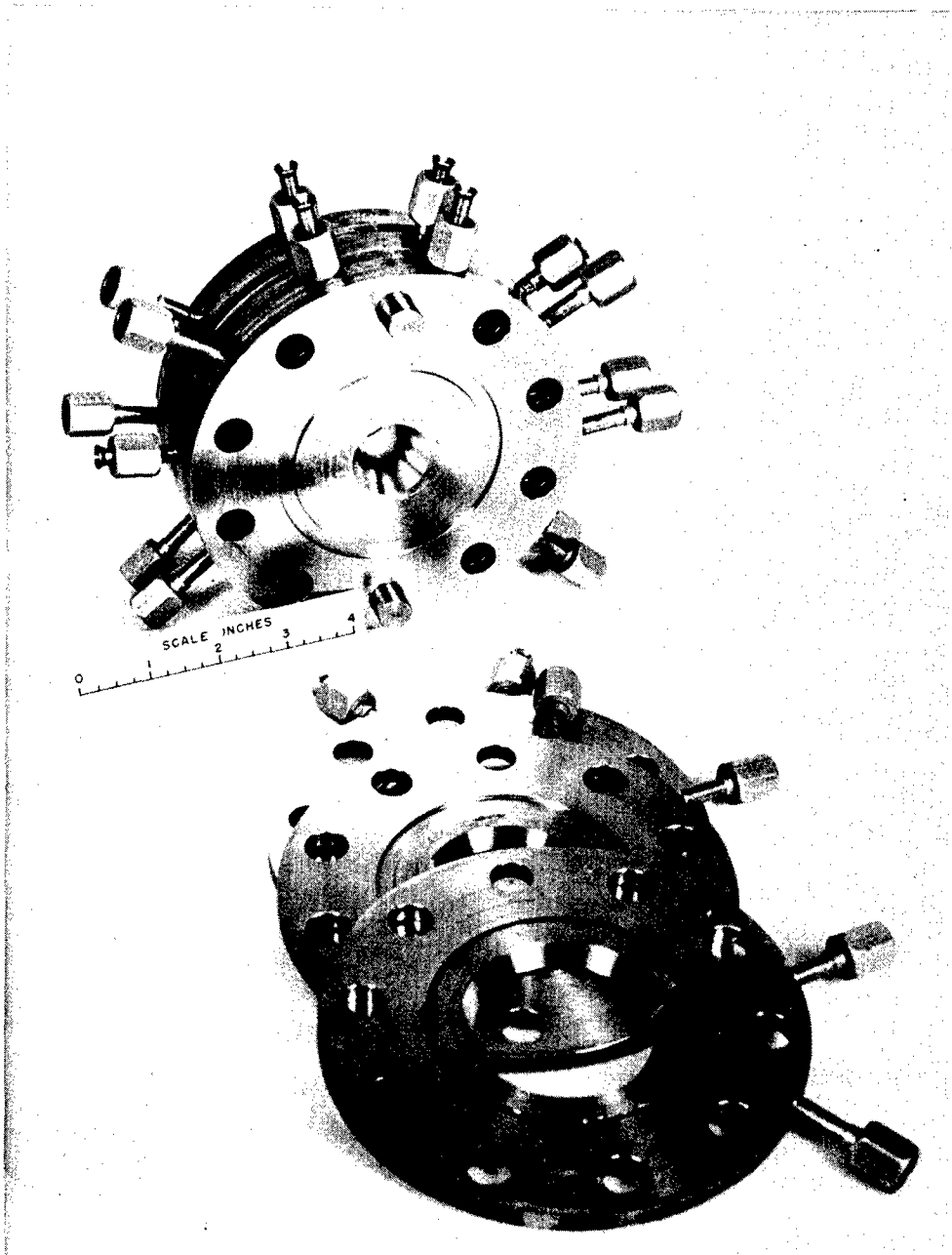

Fig. 4, Partial Assembly of First Sectional Nozzle with Indexing Pins in Place

A second nozzle was designed; this nozzle proved successful and was used for the remainder of the program. Figure 5 presents an assembly drawing of the second nozzle. The nozzle was made with a one piece inner nozzle wall and the heat flux measurements were made by dividing the coolant flow to the nozzle into six separate flows. The coolant passages consisted of channels machined integrally with the nozzle wall; the upper boundary of the coolant passage was formed by a stainless steel retaining band approximately 3/8 inch thickness. The retaining bands were welded into the coolant passage to provide a water-tight seal and also to increase the structural rigidity of the nozzle. Figure 6 shows the nozzle attached to the combustion chamber of the rocket motor.

Both nozzles were constructed from type 321 stainless steel; the nozzle exit area was selected such that the exhaust gas had a pressure slightly higher than atmospheric pressure (underexpanded) at the exit plane.

Figure 7 presents the rocket motor and its control system. The main components of the motor and its associated control equipment are described briefly in the following paragraphs.

Convectively Cooled Combustion Chamber

The convectively cooled combustion chamber was fabricated from type 347 stainless steel and consisted of an inner liner surrounded by a helical cooling passage and an outer shell. The coolant velocity in the coolant passage was approximately 52 fps at design conditions. The length to diameter ratio of the chamber was 2.0, and the inner diameter of the chamber was 2.37 inches.

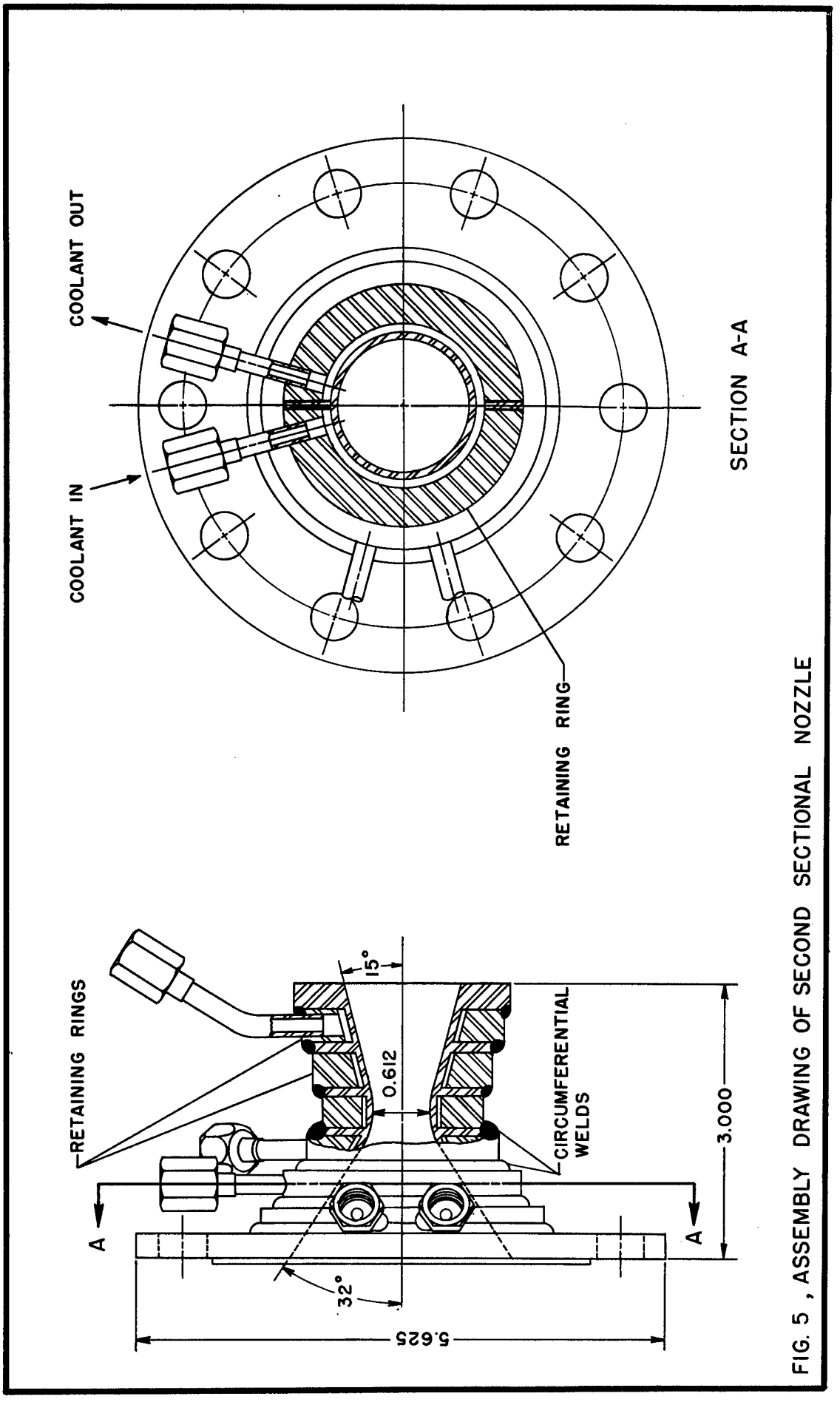

FIG. 5 , ASSEMBLY DRAWING OF SECOND SECTIONAL NOZZLE

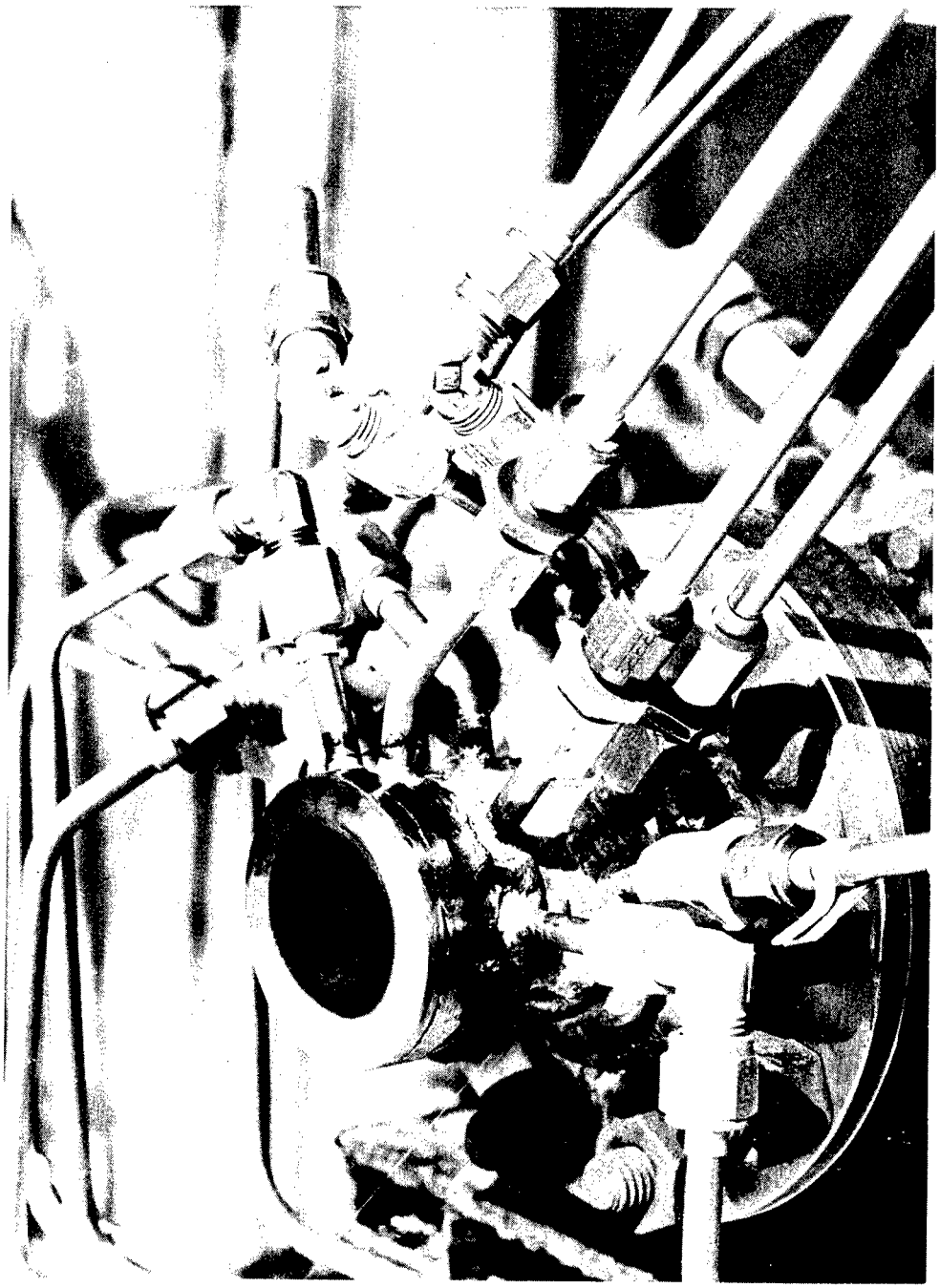

Fig. 6, Second Sectional Nozzle Attached to Combustion Chamber

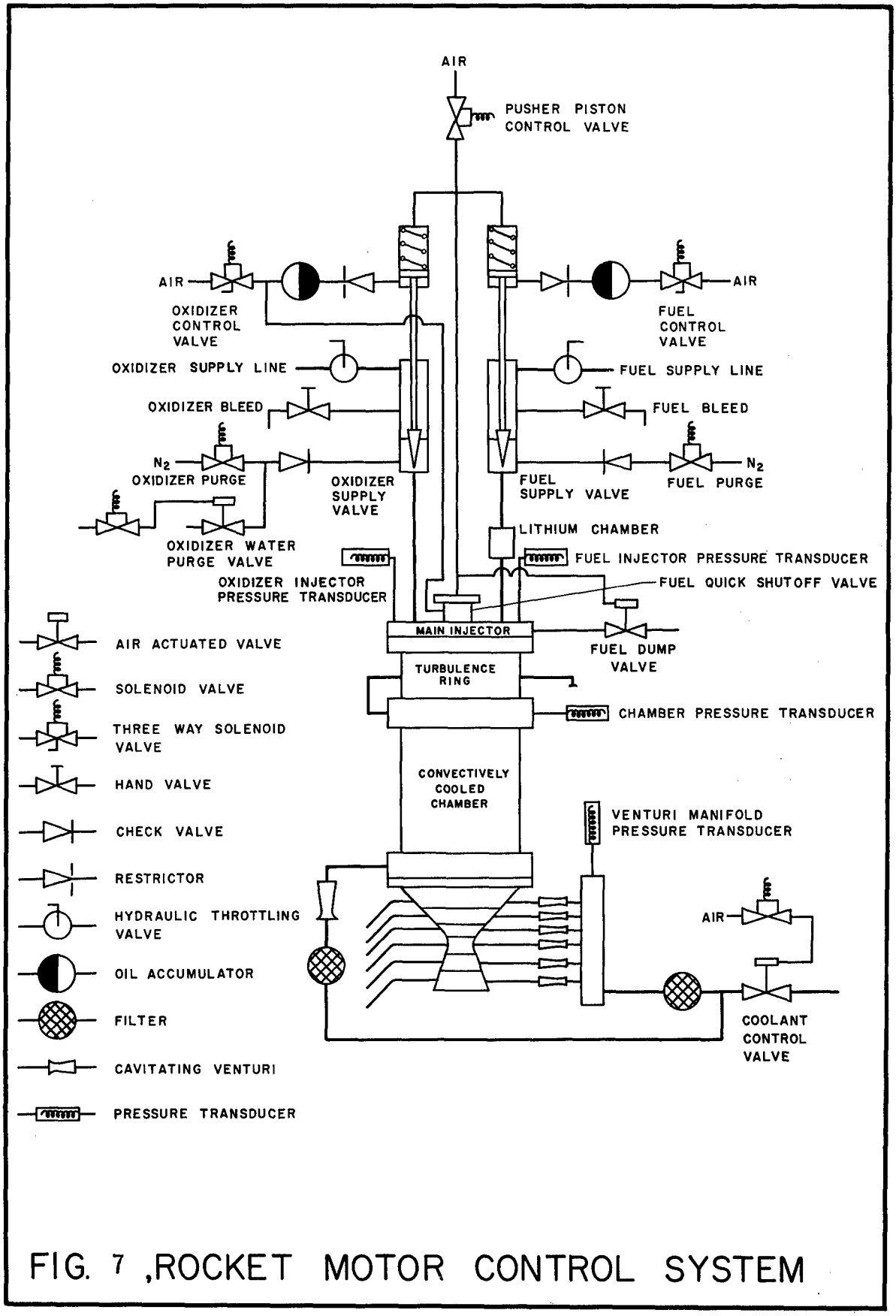

FIG. 7 ,ROCKET MOTOR CONTROL SYSTEM

Injector

A triplet type injector* having six impingement points, was used throughout the investigation. To reduce the effect of injection pattern on the heat transfer rates, the injector was used in conjunction with a turbulence ring. Figure 8 is a photograph of the injector and turbulence ring. Figure 9 shows the fuel and oxidizer injector pressure drops as a function of mixture ratio.**

Bipropellant Valve

The components of the bipropellant valve are shown in the upper section of Fig. 7. The oxidizer and fuel sides of the valve were hydraulically actuated and could be operated independently of each other. On the left and right hand sides of the spring loaded actuating cylinders are shown the three way solenoid valves, oil accumulators, and restrictors. The opening time of each side of the valve was regulated by the restrictors which were in series with the accumulators. The restrictors consisted of a check valve with a 0.0135 in hole drilled in the poppet of the check valve. This arrangement gave restricted flow at opening and full flow at shutdown. The valve pintles and valve body were taken from an Aerojet 5000 lb thrust JATO unit.

To provide an acid lead, which is desirable to reduce the possibility

---

* At each impingement point, two streams of oxidizer impinged on a single stream of fuel; impingement occurred approximately 1/2 in downstream of the injector face. With this type of injection system, the resultant momentum of the fuel and oxidizer streams is directed along the axis of the combustion chamber regardless of the relative magnitude of the oxidizer and fuel flow rates.

** lbs oxidizer/lb fuel

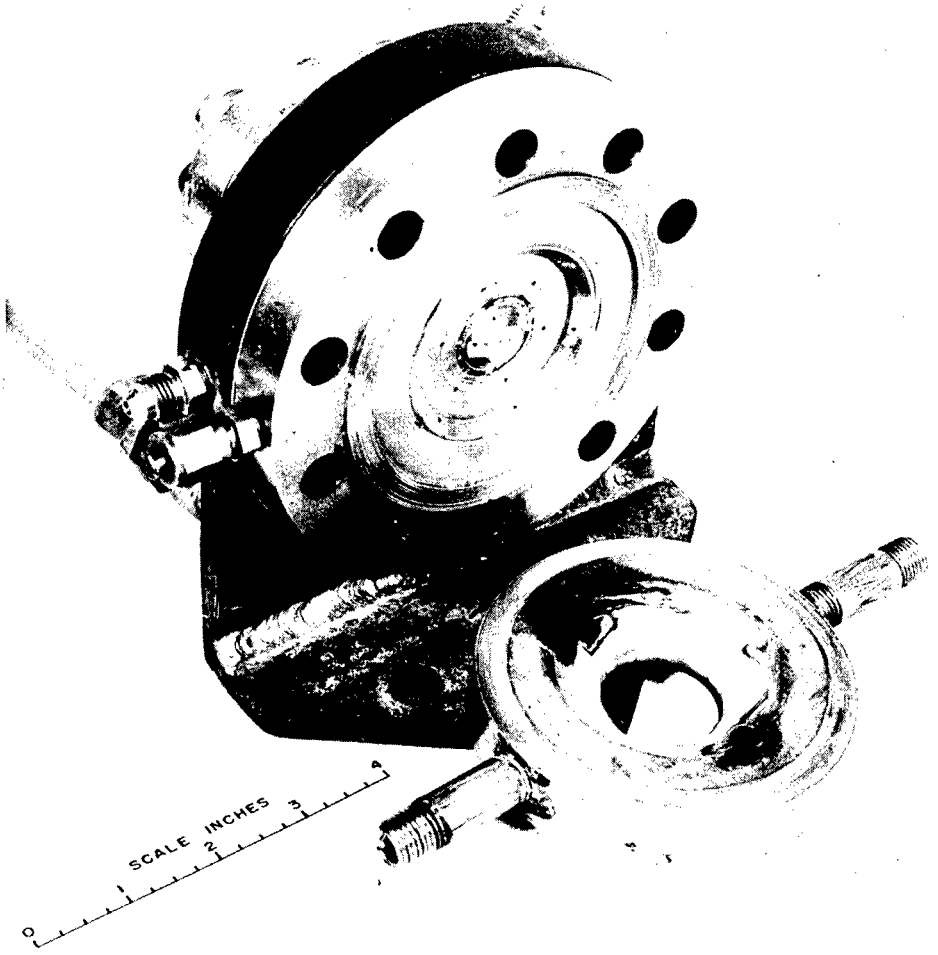

Fig. 8, Injector and Turbulence Ring

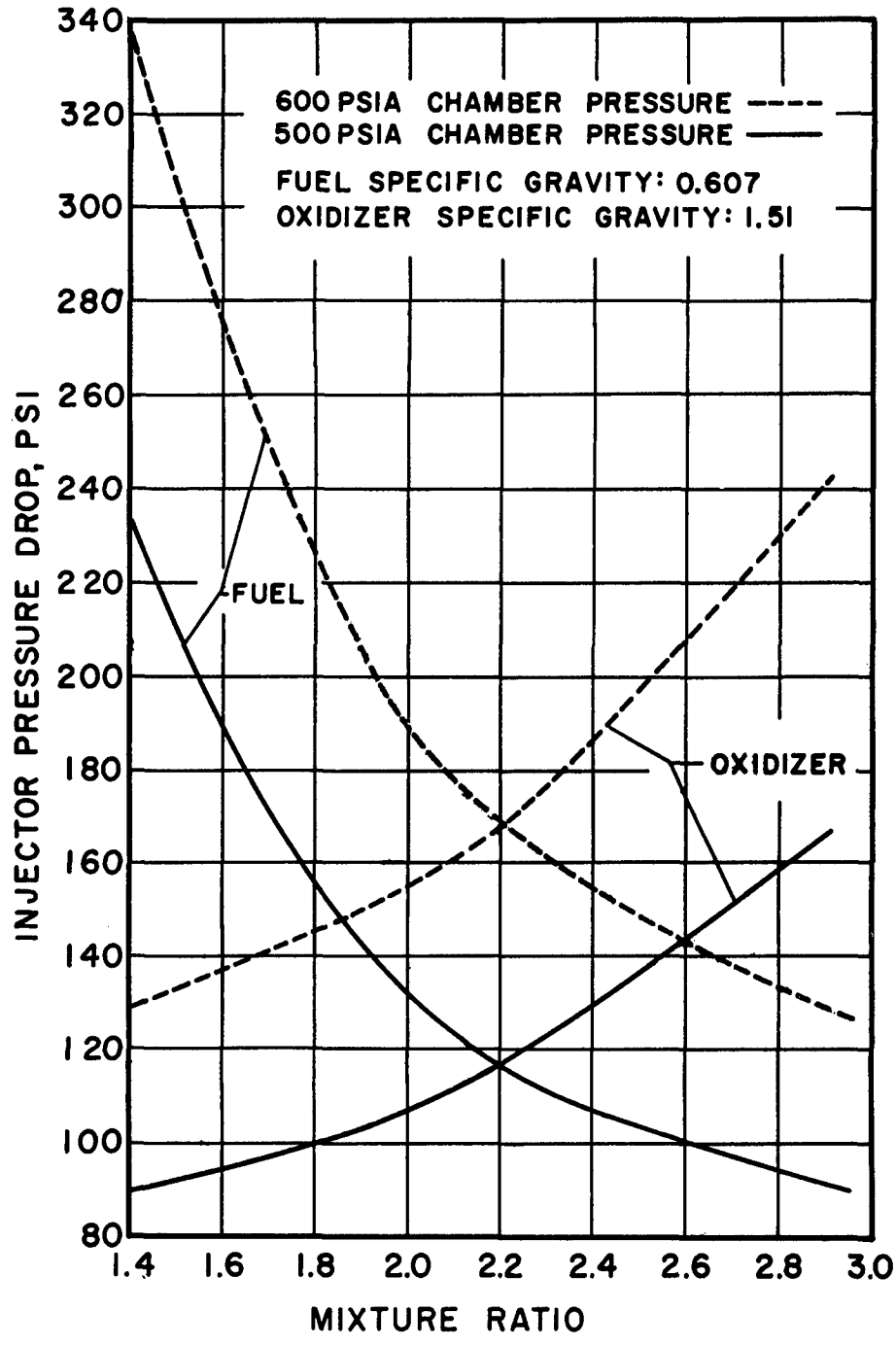

FIG. 9, VARIATION OF INJECTOR PRESSURE DROP WITH MIXTURE RATIO

of an explosive start, an electronic time delay circuit was utilized. The time delay circuit is discussed in detail in reference 6. The circuit was designed so that when the fire switch was actuated a relay immediately energized the oxidizer opening solenoid; the fuel delay was accomplished by connecting a resistance capacitance network onto the grid of a thyratron gas tube which in turn supplied voltage to a relay acting as an on-off switch to the fuel supply solenoid valve. Prior to the first run, cold start tests were conducted under simulated run conditions and the resistor in the resistance capacitance network was adjusted to give an acid lead of 0.2 sec. This lead has been shown to be satisfactory by previous experience at the Purdue University Rocket Laboratory.

Lithium Chamber

It was necessary to introduce an agent which made the propellant combination ignite on contact (hypergolic). This was done by inserting a lithium chamber, shown in Fig. 7, in the fuel line between the injector and bipropellant valve. Approximately 6 inches of lithium wire 3/32 in in diameter was used for each run; in all cases, a smooth start was obtained.

Purge System

The nitrogen purge system, indicated in Fig. 7, was designed to extinguish the flame more rapidly on shutdown, and for purging propellants which may have accumulated in the injector system. Following the nitrogen purge, the acid side of the system was purged with water.

Auxiliary Cutoff Valves

As an additional safety precaution, a quick shutoff valve was pro-

vided for the fuel side of the injector. This valve was opened and closed simultaneously with the acid side of the bipropellant valve by utilizing the same actuating air pressure. At shutdown, the bipropellant valve actuating air pressure also opened a dump valve and the fuel remaining in the short line between the injector and bipropellant valve was dumped. If the motor had been damaged so that the fuel flow could not be cut off at the thrust stand, it was possible to shut an air actuated emergency shut-off valve at the fuel tank outlet.

Cooling System

Water was used as the coolant for both the nozzle and convectively cooled chamber during all of the test runs reported herein. The coolant flow rates were controlled and measured by seven cavitating venturis* of different sizes. The venturis were designed and calibrated for use with a water tank pressure of 1000 psig. One venturi supplied chamber coolant at the rate of 1.05 lbs/sec, at 1000 psig manifold pressure, and the remaining six venturis supplied coolant to the nozzle test sections. The nozzle flow rates varied from a minimum of 0.207 lbs/sec at the second test section to a maximum of 0.536 lbs/sec in the throat section for the manifold pressure of 1000 psig. The ratio of controlled back pressure (that pressure at which cavitation ceases) to the upstream total pressure (control point) varied from 0.54 to 0.70 for the venturis used. Before the first run, the pressure drop across each section was measured and compared with the control point of each venturi; it was found that all of the venturis were operating well within the cavitation limit. To minimize the

---

* A detailed description of cavitating venturis can be found in reference 10.

pressure difference between the coolant passage and the combustion chamber and to increase the upper limit of nucleate boiling for the coolant, an orifice was inserted at the chamber coolant outlet; throttling orifices were not employed at the exit of the nozzle passages because the pressure drop of the passage of each section provided sufficient back pressure. The chamber and nozzle coolant was supplied from two tanks with a total capacity of 1150 lbs of water.

Thrust Stand

The thrust stand consisted of a four bar linkage supported on ball-bearing pivot joints (3). Loops were incorporated in the lines to minimize the hysteresis in the calibration and run points. A system was provided for thrust calibration.

Propellant Tanks

The propellant tanks were constructed from AISI type 347 stainless steel and were equipped with suitable pressurizing and vent valves. The propellant capacity was 330 lbs of WFNA and 135 lbs of NH_3.

Instrumentation

Heat Transfer and Performance Parameters

During each run, the following parameters were determined:

1) Thrust
2) Combustion pressure
3) Oxidizer flow rate
4) Fuel flow rate

5) Oxidizer injection pressure

6) Fuel injection pressure

7) Venturi manifold pressure

8) Ammonia orifice temperature

9) Chamber coolant outlet temperature

10) Nozzle coolant temperature rises

Electrical signals proportional to the above items were recorded on Minneapolis Honeywell automatic recording potentiometers, and items 2, 3, 4, 5, and 6 were also recorded simultaneously on a Consolidated Engineering Recording Oscillograph. Milliammeters located on the control panel indicated the parallel electrical output of items 2, 3, and 4 and were used during the run to indicate the propellant flow rates and combustion pressure.

Pressure and Thrust Measurement

All differential and static pressures were measured utilizing Wiancko reluctance type transducers. The thrust developed by the motor was measured by employing a Wiancko force pickup. Before each run, the differential pressure transducers were calibrated by means of a dead weight tester and the static pressure pickups were calibrated, with air pressure, against a standardized Heise gage (least count of 5 psi). The thrust pickup was calibrated with weights which were placed on a platform connected by means of a lever arm to the thrust stand. The propellant flow rates were calculated from the measured pressure drop across sharp-edged orifices located in the propellant lines. The orifice pressure drops were measured by means of the differential pressure transducers.

Temperature Measurements

The chamber coolant outlet temperature and ammonia orifice temperature (necessary for calculation of the fuel density) were measured by thermocouples and were recorded on two Minneapolis Honeywell recorders which had been previously calibrated to measure absolute temperatures.

Measurement of the nozzle coolant temperature rise by recording the inlet and outlet temperatures separately and computing the difference was considered unsatisfactory; in some cases the difference was as small as 10 F; therefore, the inlet and outlet thermocouple voltages were connected in opposition so that the net EMF was proportional to a temperature rise. A thermocouple reading of the net EMF of each thermocouple pair could be taken every 1.5 sec with the aid of a stepping switch. A schematic diagram of the thermocouple circuit and a photograph of the stepping switch is shown in Figs. 10 and 11.

Each thermocouple pair was calibrated with respect to a reference temperature of 65 F (the average coolant inlet temperature) using a Minneapolis Honeywell Recorder with a full scale deflection of 2.5 mv. Prior to the thermocouple calibration, the recording instrument was calibrated against a Leeds and Northrup Wenner Standardizing potentiometer; the potentiometer output could be set to the nearest micro-volt. The thermocouples were calibrated against a precision thermometer having a least count of 0.2 F. The thermocouple output at a particular temperature fell approximately 1.5 per cent below the values recommended by Leeds and Northrup (15). Since the readings of all the thermocouples were consistent, only one calibration curve (Fig. 12) was necessary.

The thermocouples were installed so that the coolant water was made

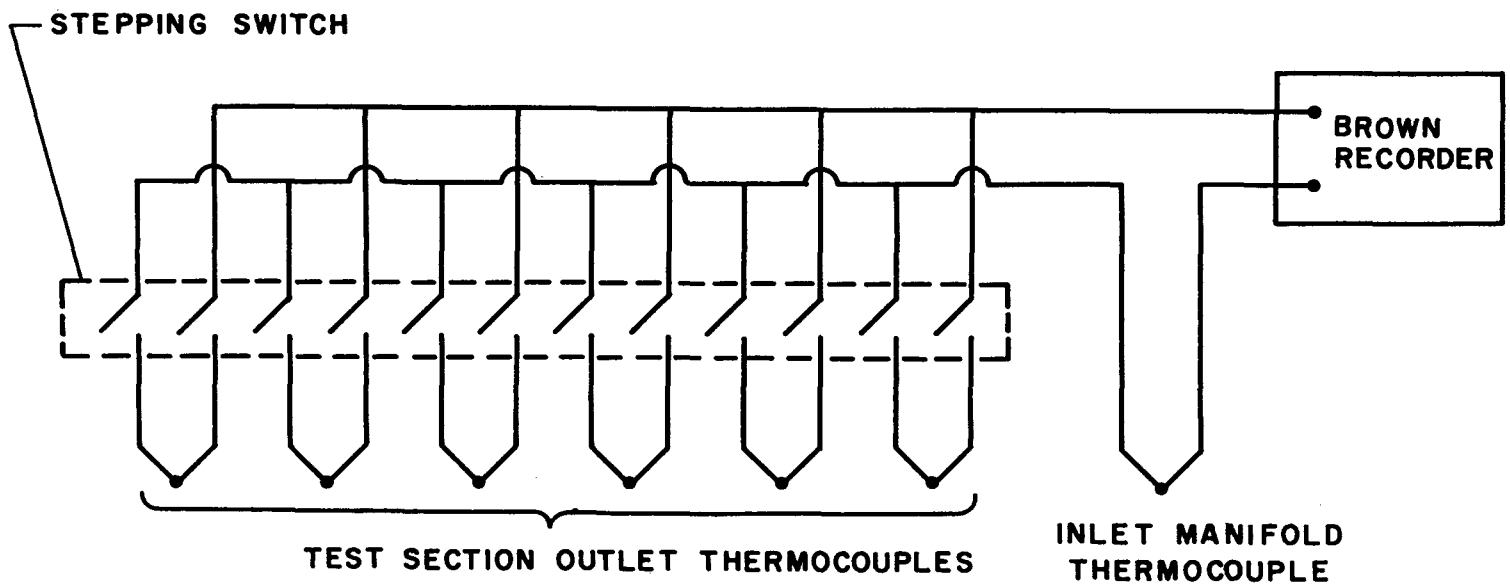

FIG. 10, SCHEMATIC DIAGRAM OF THERMOCOUPLE CIRCUIT

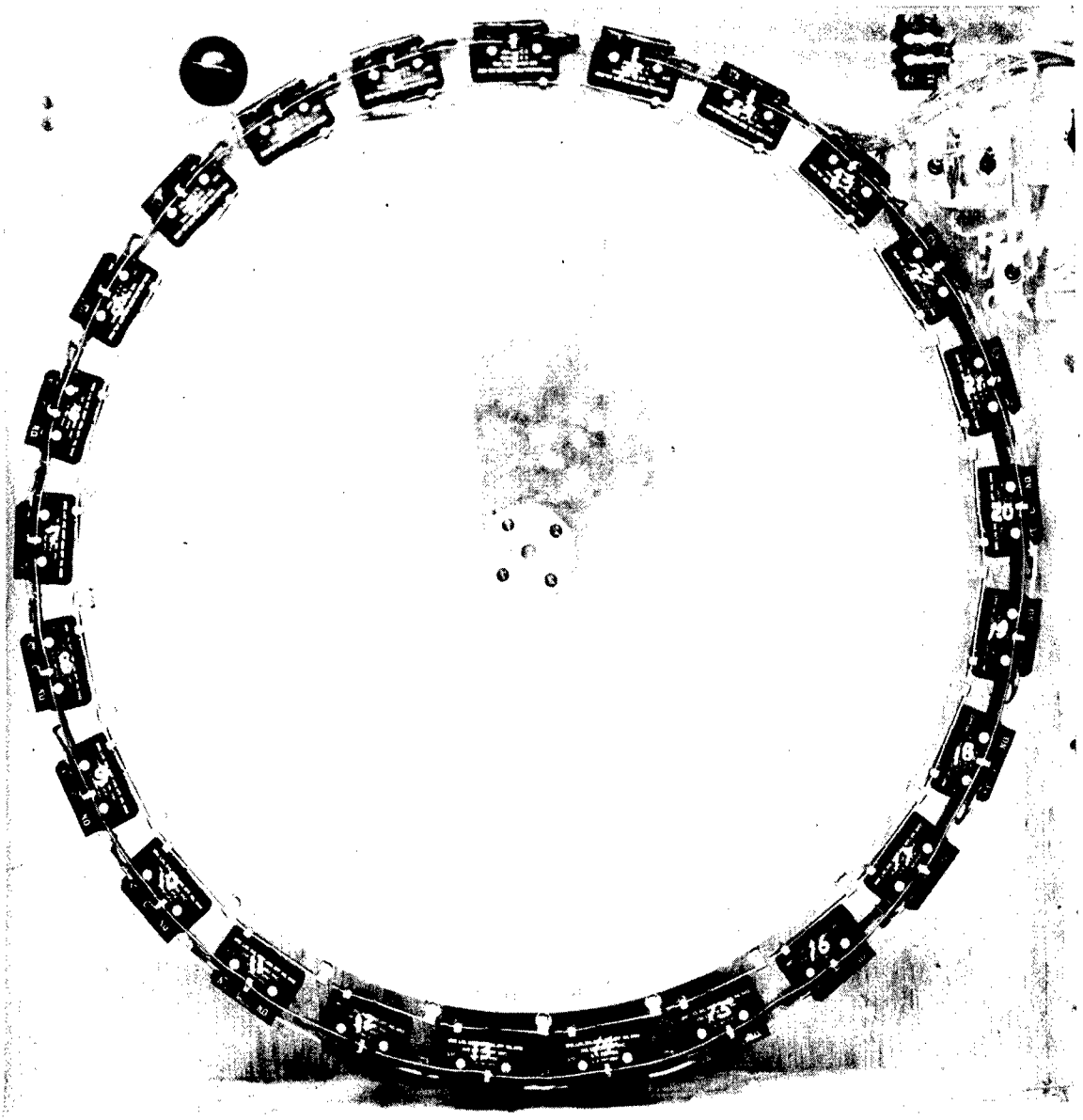

Fig. 11 Thermocouple Stepping Switch

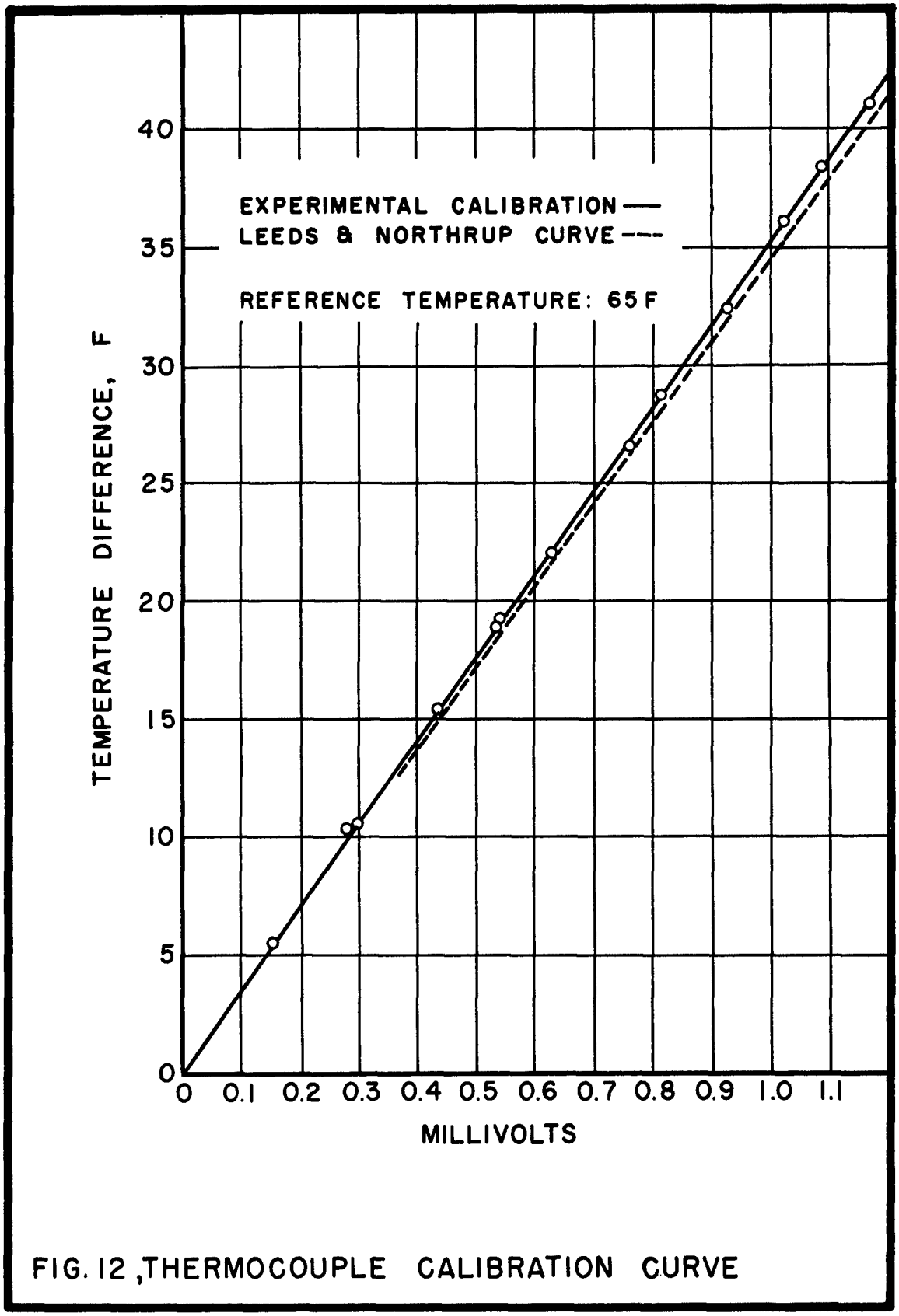

FIG. 12, THERMOCOUPLE CALIBRATION CURVE

to flow axially along the leads for approximately 1 1/2 inches; this arrangement minimized conduction errors from the thermocouple junction. Calculations were made for the heat loss from the coolant as it flowed from the test section outlet to the thermocouples and, under the worst loss conditions, the maximum error in measurement of the temperature could not have exceeded 0.5 per cent.

EXPERIMENTAL RESULTS

Heat Transfer

Heat transfer data were obtained with the water-cooled sectional nozzle of the rocket motor operating with the NH_3-WFNA propellant combination over the following range of variables:

1)	Combustion pressure	477	to	999 psia
2)	Thrust of rocket engine	196	to	433 lbs
3)	Mixture ratio	1.40	to	2.97
4)	Combustion gas temperature	2930	to	3990 F
5)	Heat flux	0.99	to	8.17 $\frac{\text{Btu}}{\text{sec in}^2}$
6)	Reynolds number (diameter)	$2.88(10)^5$	to	$15.8(10)^5$

The heat transfer results obtained with the sectional nozzle are presented in Table 3 of Appendix 3. Also included in Appendix 3 is a detailed sample calculation of the heat transfer results for a typical run.

Figure 13 presents the experimentally determined Nusselt numbers as a function of the Reynolds and Prandtl numbers for the sectional nozzle. The physical properties in the Nusselt, Reynolds, and Prandtl groups were evaluated at the arithmetic mean* film temperature. The heat transfer results for each section are indicated on the figure. In sections 1, 2, and 3, which are the sections closest to the combustion chamber, the experimental Nusselt numbers are corrected for gas radiation as described in Appendix 3. Figure 14 presents the experimental heat flux distribution in

---

* The arithmetic mean temperature is defined as the average of the free stream static temperature and the wall temperature.

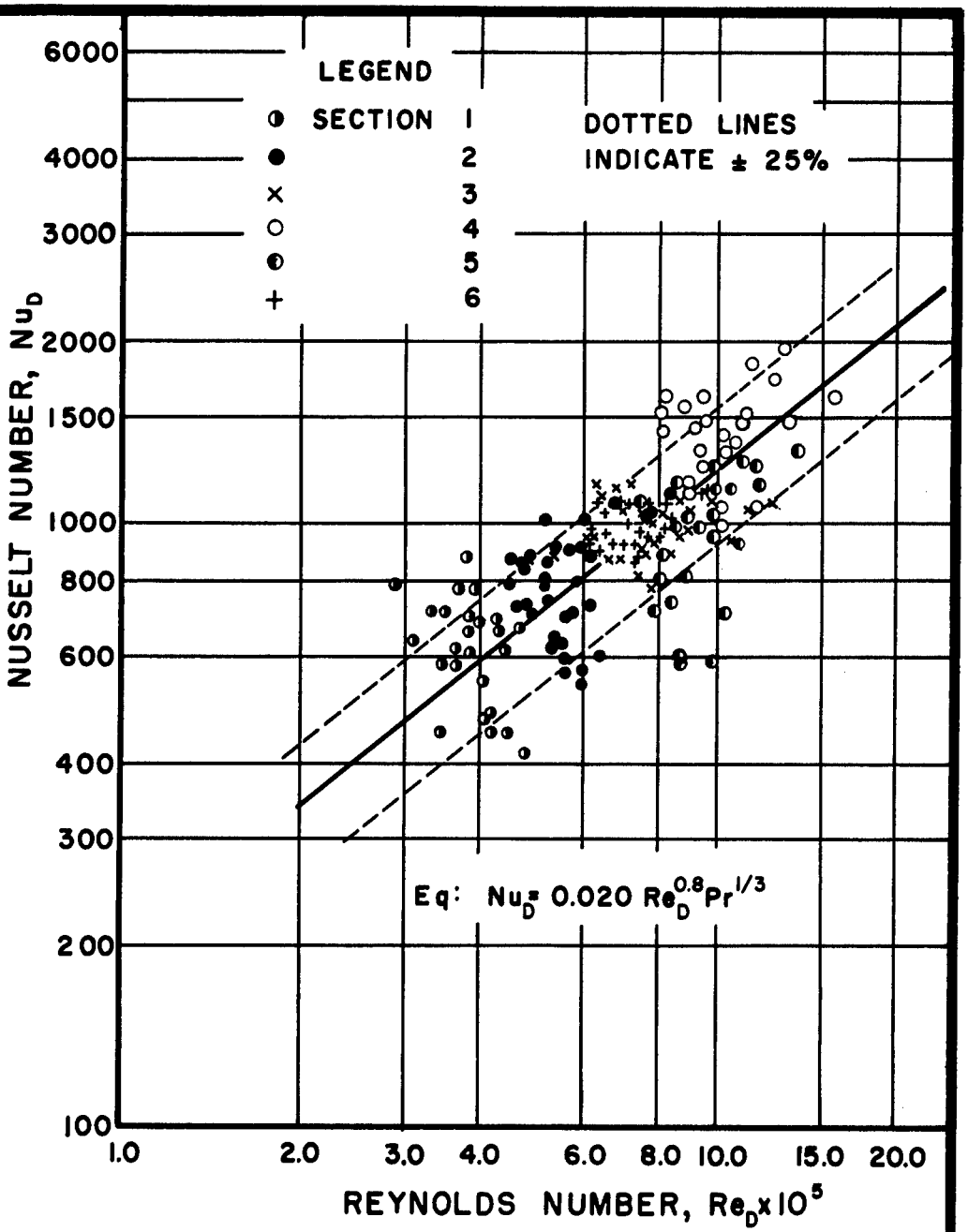

FIG. 13 ,CORRELATION OF EXPERIMENTAL NUSSELT NUMBER

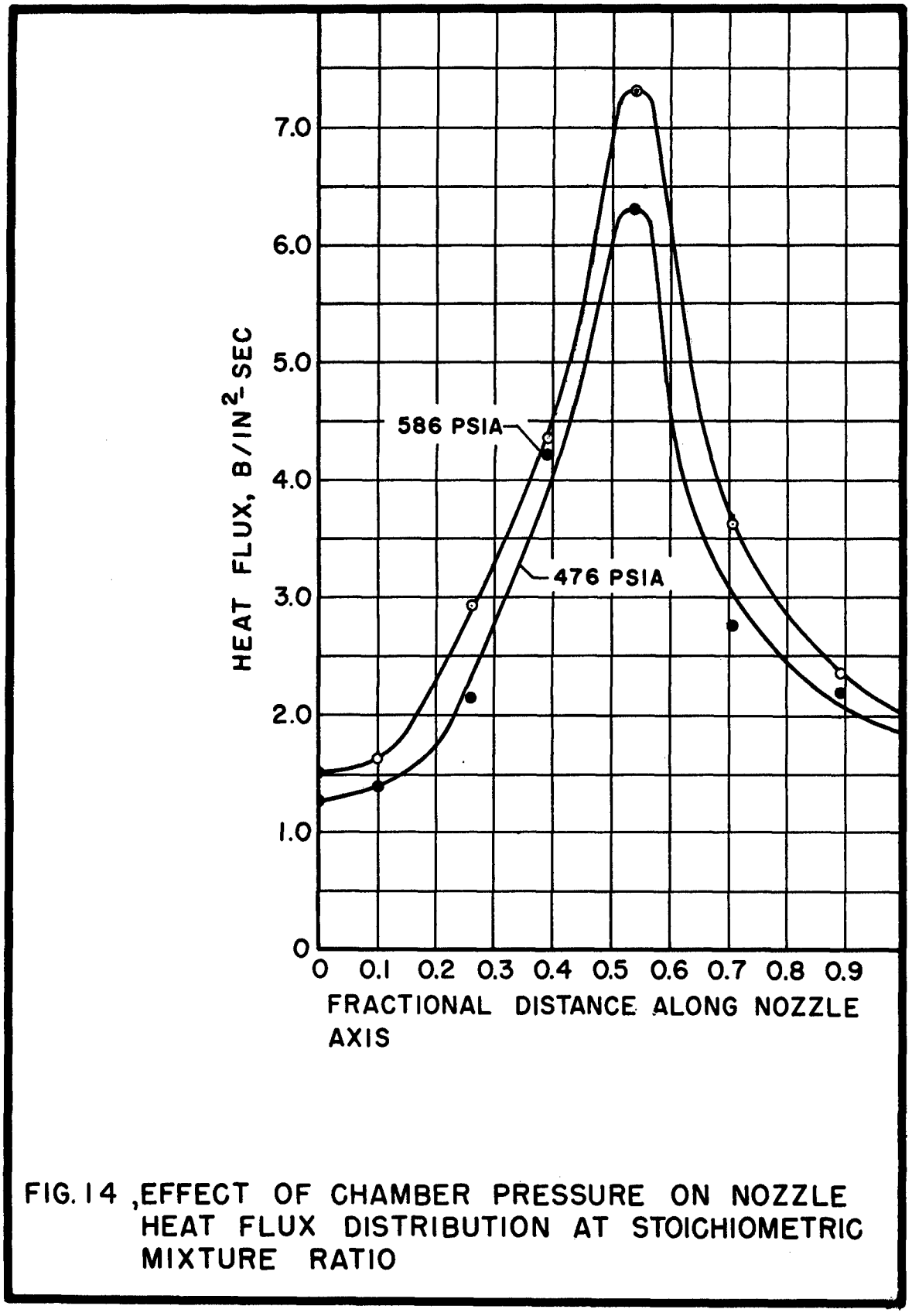

FIG. 14 ,EFFECT OF CHAMBER PRESSURE ON NOZZLE HEAT FLUX DISTRIBUTION AT STOICHIOMETRIC MIXTURE RATIO

the sectional rocket nozzle for the stoichiometric mixture ratio of runs 5 and 12.* The values obtained are typical for all of the runs and indicate not only the large values of heat flux that are obtained at the nozzle throat but also the effect of combustion pressure on the heat flux distribution.

Figure 15 presents the experimentally determined heat flux and the values of heat flux calculated from the theoretical equations (1)(2)(21). Figure 16 presents the calculated and experimentally determined values of wall temperature. Comparison of the experimental and theoretical values was made for similar gas flow conditions.**

Data obtained from runs 13 and 14 indicated that local values of the heat flux at a particular nozzle test section increased with increasing combustion pressure. The largest percentage increases in the heat flux occurred in Sections 1 and 2, and the smallest at the nozzle throat. For Sections 1 and 2, the heat flux at 1000 psia combustion pressure was approximately 45 per cent higher than the average heat flux for all of the runs at 500 psia combustion pressure. Over the same range of combustion pressures, the throat heat flux increased by only 17 per cent.

---

* As previously indicated the mixture ratio was varied during each rocket run.

** Heat transfer calculations were made for a combustion pressure of 600 psia and a mixture ratio of 2.22 (stoichiometric). The results are compared with the average experimental values for approximately 600 psia combustion pressure and stoichiometric mixture ratio. The complete calculations are presented in Reference 27, Appendix 5.

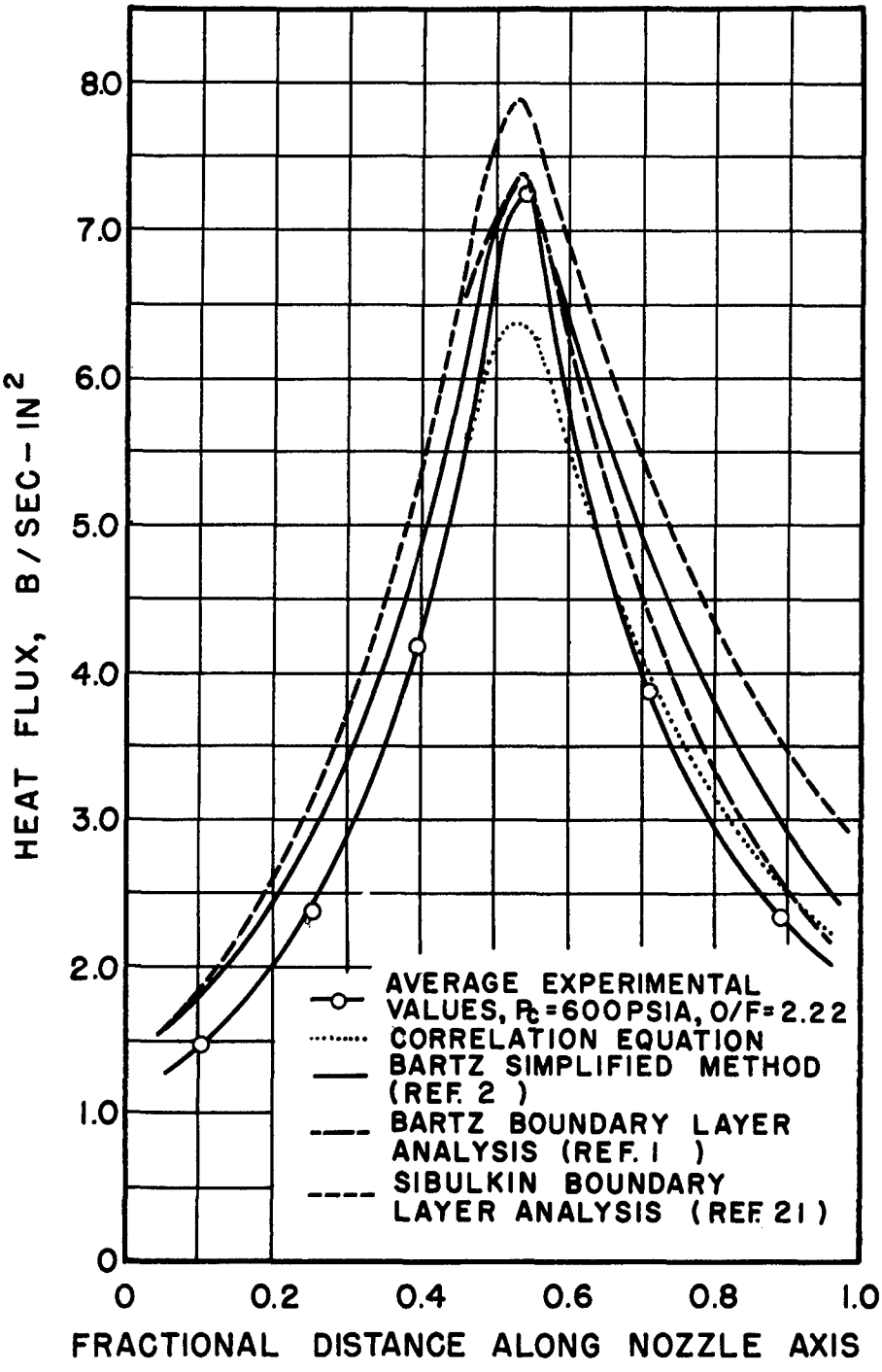

FIG. 15, CALCULATED AND EXPERIMENTAL HEAT FLUX DISTRIBUTION

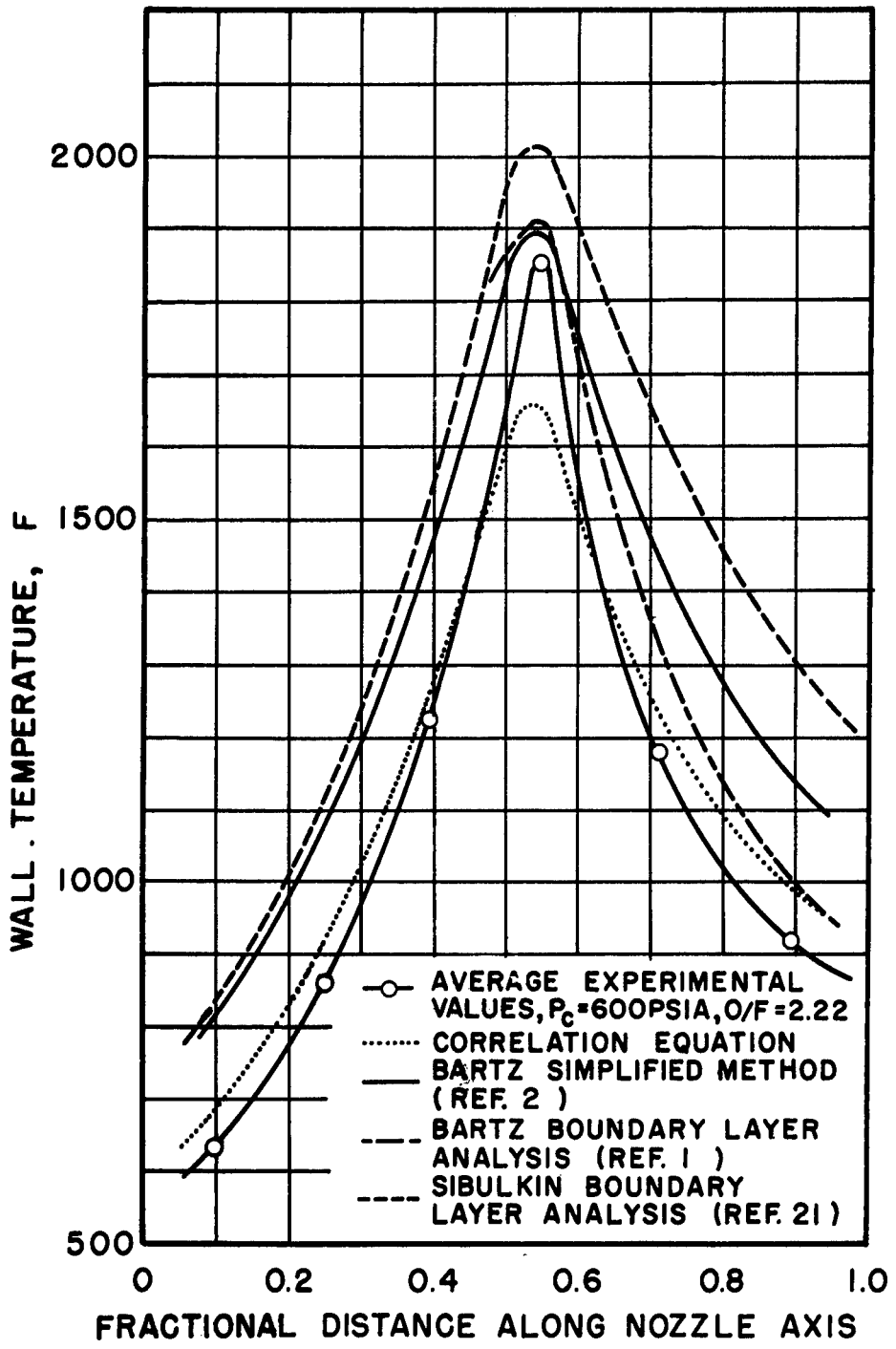

FIG. 16, CALCULATED AND EXPERIMENTAL WALL TEMPERATURE DISTRIBUTION

Performance

Rocket motor performance data and results are tabulated in Table 4 of Appendix 3. Experimental values of the specific impulse (corrected for heat transfer and deviations from the nominal chamber pressure), thrust coefficient, and characteristic exhaust velocity at 500 and 600 psia combustion pressure are plotted as functions of the mixture ratio in Figs. 17 and 18. The theoretical (frozen equilibrium)* performance is indicated on the figures.

The maximum experimental values of the specific impulse (corrected), thrust coefficient, and characteristic exhaust velocity occur at a mixture ratio of approximately 2.0 (slightly fuel rich). At 500 psia the values are

$$I_{spc} = 223 \text{ sec}$$
$$C_F = 1.43$$
$$C^* = 4910 \text{ fps}$$

and at 600 psia

$$I_{spc} = 227 \text{ sec}$$
$$C_F = 1.44$$
$$C^* = 5070 \text{ fps}$$

---

* The frozen equilibrium specific impulse is that value of specific impulse which would be obtained by a rocket motor if the composition of the combustion gas remained constant during the expansion process.

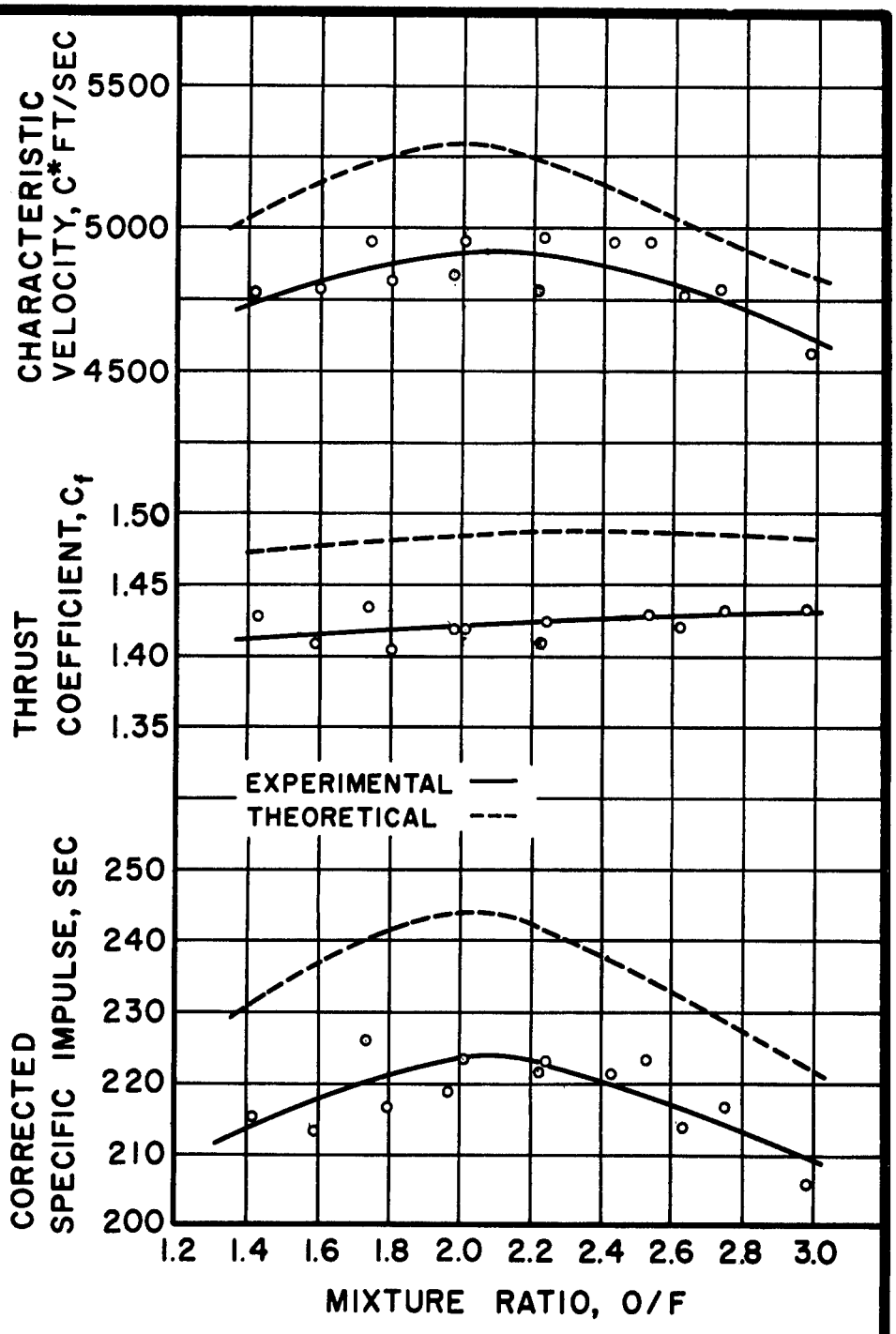

FIG. 17 ,VARIATION OF PERFORMANCE PARAMETERS WITH MIXTURE RATIO AT 500PSIA CHAMBER PRESSURE

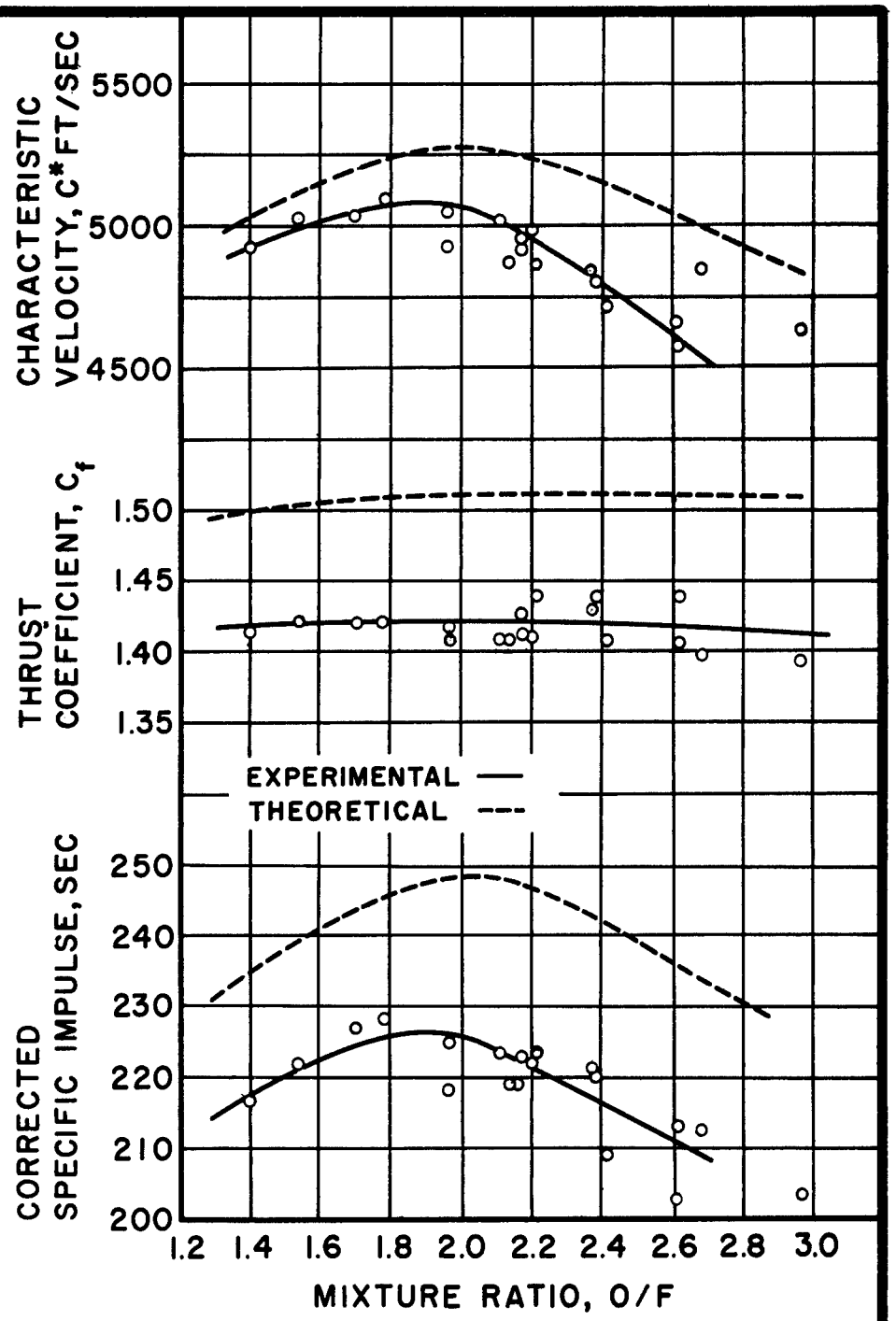

FIG. 18 ,VARIATION OF PERFORMANCE PARAMETERS WITH MIXTURE RATIO AT 600 PSIA CHAMBER PRESSURE

DISCUSSION OF EXPERIMENTAL RESULTS

Heat Transfer

Correlation of Experimental Heat Transfer Results

The heat transfer results presented in Fig. 13 apply to the hot gas film coefficient and were correlated by the equation

$$Nu_D = 0.020\ Re_D^{0.8}\ Pr^{1/3} \qquad (1)$$

where the characteristic length is the local nozzle diameter and the physical properties are evaluated at the arithmetic mean film temperature.

The exponent of the Reynolds number was chosen to be 0.80* and the Prandtl number exponent was selected as 1/3. Utilizing these exponents the constant coefficient was calculated for each combination of Nusselt, Reynolds and Prandtl numbers and the numerical average was selected as the best fit.

If the Nusselt number at the throat is calculated from equation 1 the value is too low. If only the throat Nusselt numbers are used to calculate the constant coefficient of equation 1, the coefficient in the dimensionless correlation is 0.023. It should be noted that, while the heat transfer results for Sections 1, 2, 3, and 6 (see Fig. 13) seemed to oscillate about the line representing the correlation equation, the re-

---

* The exponent of 0.80 has been shown to be satisfactory for many gases (16). Calculations based on new experimental heat transfer results for heat transfer at high temperature differences between the gas and wall indicate the value should be 0.77 (25).

sults at Section 4 (throat) were high, as previously indicated, and the values of Section 5 (immediately downstream of the throat) were consistently low. The low values of Section 5 might be explained on the basis of throat geometry. It was found that, due to machining difficulties, a cylindrical section approximately 3/16 in long was present in the throat section. Without a smooth radius of curvature to the divergence cone, the boundary layer would tend to thicken downstream of the throat and thereby reduce the heat transfer coefficient at that point. Hence, the experimental values of the Nusselt number would be expected to be lower than the values calculated by equation 1.

The characteristic length in the Reynolds and Nusselt numbers was selected as the local nozzle diameter. Theoretically, a correlation of heat transfer coefficients where the flow is undeveloped should be made on the basis of the distance measured from the origin of the boundary layer (19) such as the leading edge of a flat plate. However, for the type of flow characteristic of rocket motor combustion chambers, it is virtually impossible to establish an effective starting point for the turbulent boundary layer. Other investigators have noted (for example, reference 18)* that fully developed pipe flow correlations give results which are approximately correct.

There is considerable scatter of the Nusselt number from the correlation line. As noted in Appendix 3, the procedure employed for determining

---

* Calculations by Robison (18) show approximate agreement between the sum of calculated local values of heat flux and the overall experimental value of nozzle heat flux. In this reference the overall experimental heat flux was defined as the ratio of the total heat transferred to the coolant to the gas side heat transfer surface area.

the local gas film resistances was to calculate the overall resistance to heat flow and then subtract the calculated wall and liquid film resistances from the overall resistance. Employing that procedure, the sum of the radiation and gas film convection resistances were calculated. To separate the gas film resistance from that quantity, a radiation correction was applied as explained in Appendix 3.

In calculating the overall resistance to heat flow, the quantities which could be determined experimentally were the coolant bulk temperature and the heat flux for a nozzle test section. The adiabatic wall temperature (assumed to be the gas total temperature) was assumed to be equal to the theoretical flame temperature (calculated in reference 7) multiplied by the square of the ratio of the experimental to the theoretical characteristic velocity. The calculated wall resistance to heat flow is the ratio of the nozzle wall thickness to the thermal conductivity of the wall evaluated at the average wall temperature, and the calculated liquid film resistance is the reciprocal of the liquid film heat transfer coefficient. A correction was made for radiation extrapolation of the method commonly employed in computing radiant heat transfer in furnaces.*

Some of the scatter of the heat transfer results indicated in Fig. 13 is probably due to such factors as (a) the variation in injection pattern because of operating the motor with mixture ratios other than the design mixture ratio (stoichiometric), (b) the rough combustion encountered with low mixture ratio ($1.4 \leq O/F \leq 1.6$), probably due to the unequal injection pressure drops with those mixture ratios (see Fig. 9), and (c) the scale deposits due to contaminants in the acid.

---

* The complete calculations are presented in Reference 27.

Discussion of the Heat Transfer with High Combustion Pressures

It was indicated in the results for test runs 13 and 14 that the largest percentage increases in local heat flux due to increased combustion pressure occurred in Sections 1 and 2, while the smallest percentage increase occurred in the throat section. The larger increases of heat flux at Sections 1 and 2 may be partly explained on the basis of the relative magnitude of the convection resistance compared to the total resistance to heat flow. In Sections 1 and 2 the convection resistance comprises approximately 80 per cent of the total resistance to heat flow whereas, in the throat section, the convection resistance accounts for approximately 60 per cent of the total resistance. Hence, decreases in the convection resistance due to increases in combustion pressure are more significant in Sections 1 and 2. It is, therefore, concluded that for the same nozzle the peak of the heat flux distribution curve becomes less pronounced as the combustion pressure is increased.

Comparison of Experimental and Theoretical Heat Transfer Results

Figures 15 and 16 summarize the results of the heat transfer calculations (27). For generality, the calculated values of heat flux and wall temperature are plotted as functions of the fractional distance along the nozzle axis, and as noted previously, the averaged experimental results for similar conditions are also presented.

Figure 15 indicates that the best agreement between the analytical curves and the experimental points, is given by the correlation equation; however, at the throat the heat flux predicted by the correlation equation

is low by 12 per cent. Calculations based on Sibulkin's incompressible analysis (21) gave heat fluxes consistently higher than the experimental values and over-estimated the peak value by 8 per cent. The best prediction of the throat heat flux was by the simplified (2) and turbulent boundary layer (1) analyses of Bartz; both of Bartz's methods gave, however, calculated values consistently higher than the experimental heat flux values at all other sections of the nozzle.

Figure 16 shows the variation of the nozzle wall temperature with dimensionless axial distance. The comments made above regarding the comparison of the calculated and experimental heat flux distributions also apply to the wall temperature distributions. Wall temperatures computed by means of the correlation equation gave the best agreement for most of the calculated points; however, the calculated throat temperature was only 1660 F compared to the experimental* value of 1850 F. According to calculations employing Sibulkin's analysis, the throat temperature was 2025 F. Both the simplified and turbulent boundary layer analyses of Bartz gave throat wall temperatures which were higher than experimental by only 60 F.

Performance

At 500 psia combustion pressure the previously indicated maximum experimental values of the corrected specific impulse, thrust coefficient, and characteristic exhaust velocity are 92, 96, and 92 per cent of their corresponding frozen equilibrium values. At 600 psia combustiom

---

* It is emphasized that wall temperatures were not measured. Henceforth, the experimental value of wall temperature is meant to be wall temperatures calculated on the basis of experimental heat fluxes.

pressure the ratio of the maximum experimental values of those parameters to their theoretical values is 91, 96, and 96 per cent. The corrected specific impulse, referred to above, is that value of specific impulse which would be obtained if the experimental motor were regeneratively cooled. The method employed for calculating the correction for regenerative cooling is described in Appendix 3.

CONCLUSIONS

1. The heat flux was measured in a specially constructed nozzle and the heat flux as a function of nozzle length for two typical run points is presented in Fig. 14; the results for the other runs are presented in Table 3, Appendix 3.

2. Increasing the combustion pressure increased the heat flux. At 500 psia combustion pressure the average maximum throat heat flux was 6.65 Btu/sec in^2 at stoichiometric mixture ratio and at 1000 psia combustion pressure the maximum heat flux was 7.67 Btu/sec in^2, an increase of 15 per cent.

3. The heat transfer characteristics on the gas side of the rocket nozzle wall were calculated from the experimental data and the results were correlated by the equation

$$Nu_D = 0.020\ Re_D^{0.8}\ Pr^{1/3} \qquad (1)$$

where the characteristic dimension in the Reynolds and Nusselt numbers is the nozzle diameter, and the physical properties of the gas were evaluated at the arithmetic mean film temperature. The above equation correlates 80 per cent of the experimental data points within ± 25 per cent (see Fig. 13).

4. The average of the experimental values of heat flux and wall temperature obtained in the runs made at 600 psia chamber pressure, at stoichiometric mixture ratio, were compared with values calculated from equations obtained by three theoretical studies (1)(2)(21) and the afore-mentioned correlation equation. The results are presented in Figs. 15 and 16. The

agreement between all of the equations and the experimental results is good. The correlation equation is the best fit for all experimental points except at the throat. At the throat the equations of references 1 and 2 are more satisfactory.

5. The equation developed by Bartz in reference 2 (which assumes the primary factor affecting the convective heat transfer coefficient is the mass rate of flow per unit area and that boundary layer development plays only a secondary influence) is recommended for calculating the heat flux and wall temperature. The equation is

$$h_g = \frac{0.026}{D^{*0.2}} \left[\frac{\mu^{0.2} c_p}{Pr^{0.6}}\right]_o \left[\frac{P_c g}{C^*}\right]^{0.8} \left[\frac{D^*}{r_c}\right]^{0.1} \frac{\sigma}{\left[\frac{A}{A^*}\right]^{0.9}} \qquad (2)$$

The nomenclature is defined in Appendix 1.

This equation has some basis in theory in that the throat heat transfer coefficient (the most critical point) is matched to the more analytical analysis of reference 1. On the basis of the experimental work reported herein, the above-mentioned equation gives the best prediction of the throat heat flux and elsewhere in the nozzle yields results which are conservative in that estimates of the heat flux and wall temperatures are slightly high.

6. At 500 psia combustion pressure, in the rocket motor tested, the propellant combination WFNA-NH_3 gave a corrected specific impulse which was 92 per cent of the theoretical value based on frozen equilbrium conditions and a characteristic exhaust velocity 92 per cent of theoretical. At 600

psia combustion pressure, the corrected specific impulse and characteristic exhaust velocity were 91 and 96 per cent of the theoretical values. At both combustion pressures, the experimental thrust coefficient was 96 per cent of the theoretical values.

APPENDICES

APPENDIX 1

NOMENCLATURE

a Speed of sound (fps) or function defined by equation 5.18.

A Nozzle cross sectional area normal to the gas flow (in^2).

A_s Heat transfer surface area (in^2).

b Function defined by equation 5.19.

b' Function defined by equation 5.28.

B Function defined by equation 4.47.

C A constant, or function defined by equation 5.20.

C_F Thrust coefficient.

C_H Correction factor for liquid film coefficient due to passage curvature.

C_p Specific heat at constant pressure (Btu/lb F).

C_v Specific heat at constant volume (Btu/lb F).

C_w Correction factor for effect of pressure on gas emissivity.

C* Characteristic exhaust velocity (fps).

C' Function defined by equation 5.29.

d Nozzle wall thickness (in).

D Local nozzle diameter (in).

D_H Helix diameter of coolant passage (in).

e Brayton cycle efficiency defined by equation 3.25.

f Friction coefficient defined by equation 4.21.

F Thrust (lbs).

F(x) Function defined by equation 4.44 ($ft^{9/4}$ $fps^{27/7}$).

NOMENCLATURE (Continued)

$f(x)$, $f'(x)$, $g(x)$, $g'(x)$ Coefficients of the differential equations 4.30 and 4.38 (1/in, 1/in, $in^{1/4}$, 1/in)

g Acceleration due to gravity (32.17 ft/sec^2)

h Convection coefficient (Btu/sec in^2 F) and specific enthalpy (Btu/lb).

I_1 Definite integral defined by equation 5.15.

I_2 Definite integral defined by equation 5.16.

I_1' Definite integral I_1 with coefficients b' and c' replaced for b and c.

I_{sp} Specific impulse (sec).

I_{spc} Specific impulse corrected for heat transfer and deviations in chamber pressure (sec).

I'_{spc} Specific impulse corrected for heat transfer (sec).

j Colburn heat transfer factor.

J Mechanical equivalent of heat (778 ft lbs/Btu).

k Thermal conductivity (Btu/sec in F or Btu/hr ft F).

L Radiant beam length (ft or in).

L_o Zero partial pressure radiant beam length (ft or in).

L* Characteristic length (in).

m Hydraulic radius of coolant passage (in).

mw Molecular weight (lbs/lb mole).

M Mach number.

M* Dimensionless Mach number defined by equation 5.34.

Nu Nusselt number.

Nu_{Du}	Nusselt number based on diameter, uncorrected for radiation.
P	Pressure (psia or psfa).
P_w	Water vapor partial pressure (atm).
Pr	Prandtl number.
q	Heat transfer rate (Btu/sec).
q"	Heat flux (Btu/sec in^2).
r	Local nozzle radius (in or ft).
r_c	Throat radius of curvature (in).
R	Gas constant (ft/R or ft lbs/slug R).
Re	Reynolds number.
St	Stanton number.
T	Temperature (R or F).
t_T	Total temperature $y < \Delta$ (R or F).
ΔT	Coolant temperature rise (F).
u	Component of velocity in x direction; $y < \delta$ (fps).
U_∞	Free stream velocity (fps).
v	Component of velocity in y direction; $y < \delta$ (fps).
V	Volume of enclosure containing a mass of radiating gas (ft^3).
V_e	Effective exhaust velocity (fps).
V_{ec}	Effective exhaust velocity corrected for heat transfer (fps).
$\dot{w}$	weight flow rate (lbs/sec).

NOMENCLATURE (Continued)

x	Coordinate parallel to nozzle wall (in or ft).
x_o	Effective starting point for thermal boundary layer (in or ft), boundary condition on solution of equation 4.51.
y	Coordinate normal to nozzle wall (in).
Z	Parameter defined by equation 5.17.
α	Recovery factor, nozzle divergence half-angle (o), or absorptivity.
β	Nozzle convergence half angle (o).
γ	Specific heat ratio.
δ	Velocity boundary layer thickness (in or ft).
δ^*	Boundary layer displacement thickness, defined by equation 4.18, (in or ft).
Δ	Thermal boundary layer thickness (in or ft).
Δ^*	Thermal boundary layer displacement thickness, defined by equation 4.25 (in or ft).
ϵ	Emissivity.
ϵ_w	Water vapor emissivity.
ϵ_{wg}	Wall emissivity.
ϵ'_{wg}	Effective wall emissivity defined by equation 5.2.
θ	Boundary layer momentum thickness defined by equation 4.17 (in or ft).
λ	Boundary layer shape parameter defined by equation 4.36 or correction factor for nozzle divergence losses.
μ	Dynamic viscosity (slugs/ft hr or lbs/ in sec)

NOMENCLATURE (Continued)

ν Kinematic viscosity (ft^2/sec).

ρ Density (lbs/ft^3 or $slugs/ft^3$).

σ Stefan Boltzmann constant ($Btu/hr\ ft^2\ F^4$) or function defined by equation 4.57.

τ Time (sec) or shear stress (lbs/ft^2).

ϕ Boundary layer energy thickness defined by equation 4.24 (in or ft) or velocity coefficient.

$\dot{\Phi}$ Dissipation function ($Btu/sec\ in^3$).

Ω Thermal resistance to heat flow ($sec\ in^2\ F/Btu$).

ω Viscosity exponent defined by the relation $\mu \propto T^{\omega}$.

Subscripts

a Ambient (as P_a).

am Arithmetic mean (as T_{am}).

aw Adiabatic wall (as T_{aw}).

BL Bulk liquid (as T_{BL}).

c Convection or chamber (as q_c'' or P_c).

D Based on diameter (as Re_D and Nu_D).

f Fuel (as $\dot{w}_f$).

g Gas (as h_g).

L Liquid (as h_L).

ox Oxidizer (as $\dot{w}_{ox}$).

NOMENCLATURE (Continued)

p	Propellant (as $\dot{w}_p$).
r	Radiation (as q''_r).
T	Refers to total or isentropic stagnation state or total resistance to heat flow (as P_T or Ω_T).
Th	Theoretical (as C^*_{Th}).
w	Wall (as τ_w).
wg	Gas wall (as T_{wg}).
x	Based on x (as Re_x or Nu_x).
o	Conditions at x = o (as M^*_o) except L_o
∞	Conditions in free stream $y > \delta$ (as U_∞).

Superscript

*	Conditions at M = 1 (as A^*), except C*, L*, ξ^*, Δ^*, and M*.

APPENDIX 2

PHYSICAL AND STATE PROPERTIES OF THE COMBUSTION PRODUCTS OF WFNA - NH_3

Since the Nusselt, Reynolds, and Prandtl numbers enter into heat transfer calculations, it is necessary that the physical properties, viscosity, thermal conductivity, and Prandtl number be known or estimated. In addition the state properties, pressure, temperature, and density must also be determined.

For the correlation of heat transfer coefficients reported herein, thermal conductivity and viscosity data were extrapolated by means of the equations used to calculate the tabulated values of reference 12. The temperature limits of thermal conductivity and viscosity data, at 1 atm pressure, according to reference 12, are summarized in Table 1.

Table 1

Temperature Limits of Viscosity and Thermal Conductivity Data at 1 atm

Component	μ	k
H_2	1520 F	800 F
N_2	2240	1700
O_2	3140	620
H_2O	1520 (2240 F at 0.01 atm)	980

Values for the specific heat of the products are taken from reference 7 and cover the temperature range from 1340 to 5300 F. In the temperature

region of interest, the effect of pressure on the above properties is negligible.

The viscosity and thermal conductivity of the products were determined by taking a weighted average of the components of the gas. Although more elaborate mixing rules exist (4), it was felt that uncertainties introduced by extrapolation of the physical properties to the higher temperatures would more than offset the additional accuracy obtainable with a more exact mixing rule.

In the averaging of the properties it was assumed that the only components of importance were H_2, N_2, O_2, and H_2O. Thermochemical calculations in reference 7 showed that the concentration of the radicals O, OH, H, NO, and N was less than 2 per cent over the mixture ratios from 1.4 to 3.0 for the WFNA-NH_3 system. The concentration of the products of combustion are taken from reference 7 and are shown in Fig. 19 as a function of mixture ratio. Values of the thermal conductivity, viscosity, specific heat, and Prandtl number are plotted as a function of temperature with mixture ratio as a parameter in Figs. 20, 21, 22, and 23.

The state properties, pressure, temperature and density in the nozzle passage were determined from the one-dimensional, isentropic, compressible flow tables of reference 13 using the calculated value of chamber total temperature and the experimental total pressure. The value of the specific heat ratio at the combustion temperature varied from 1.21 to 1.24 over the range of mixture ratios 1.4 to 3.0; therefore the tables of reference 13 for $\gamma = 1.20$ were used. Of the above state properties the most important in the analysis of heat transfer characteristics is the gas static temperature, T_∞ .

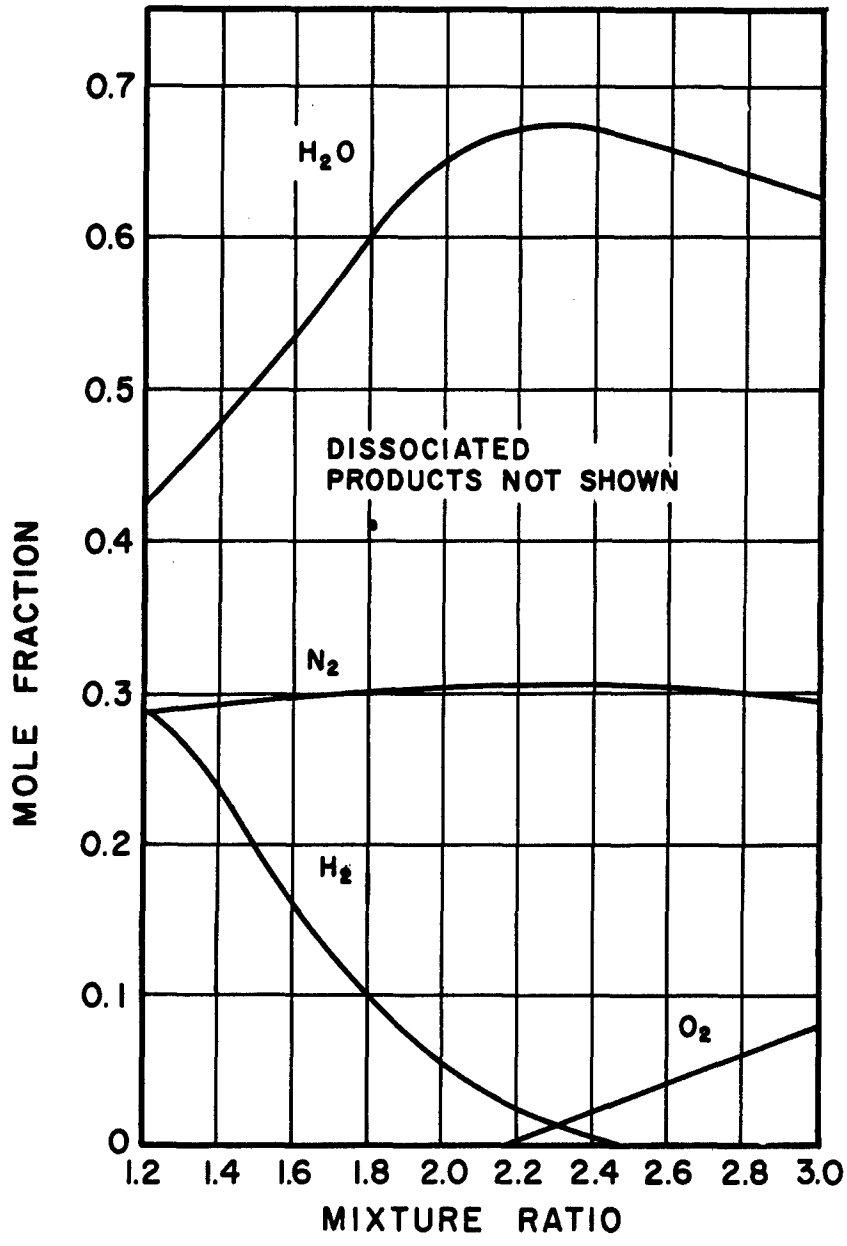

FIG. 19 ,VARIATION OF EQUILIBRIUM COMPOSITION OF COMBUSTION PRODUCTS OF NH_3 -WFNA WITH MIXTURE RATIO

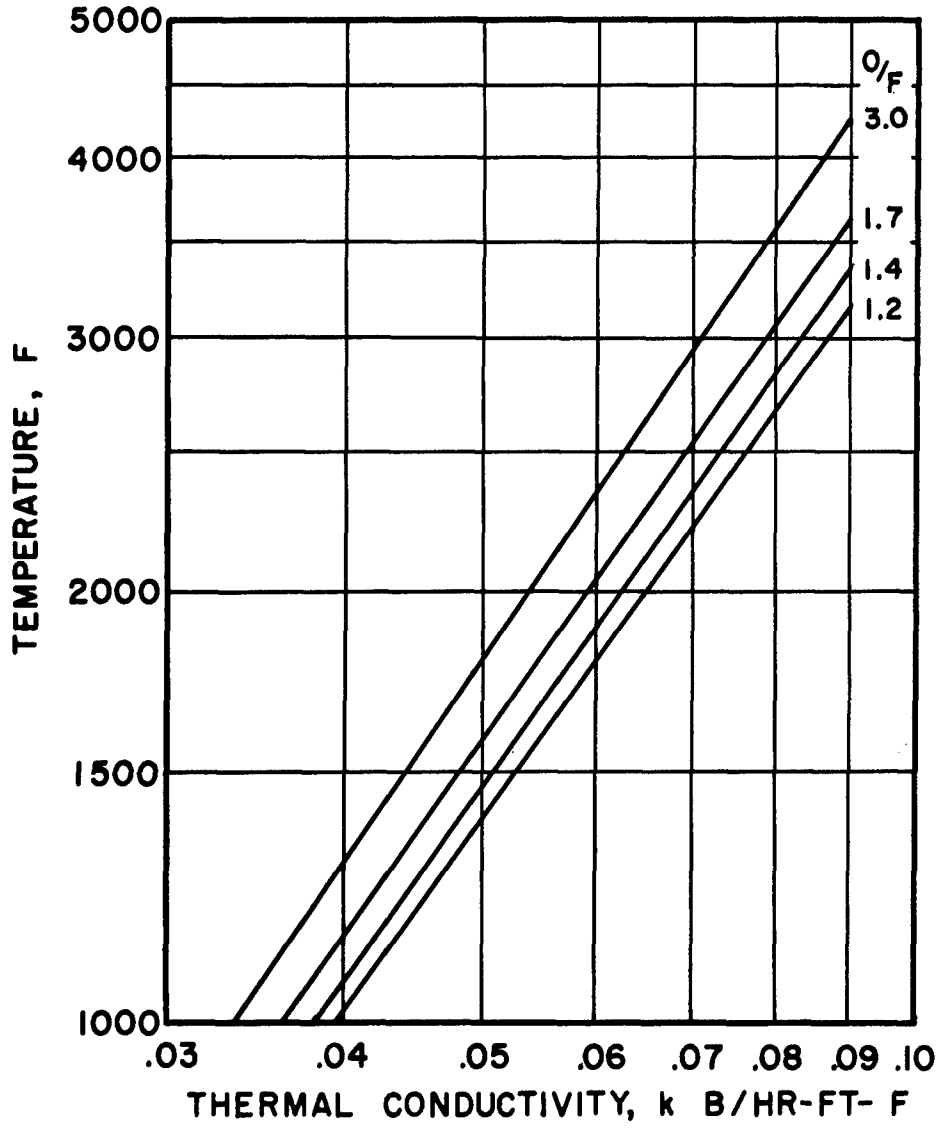

FIG. 20, VARIATION OF THERMAL CONDUCTIVITY OF COMBUSTION PRODUCTS OF NH_3-WFNA WITH TEMPERATURE

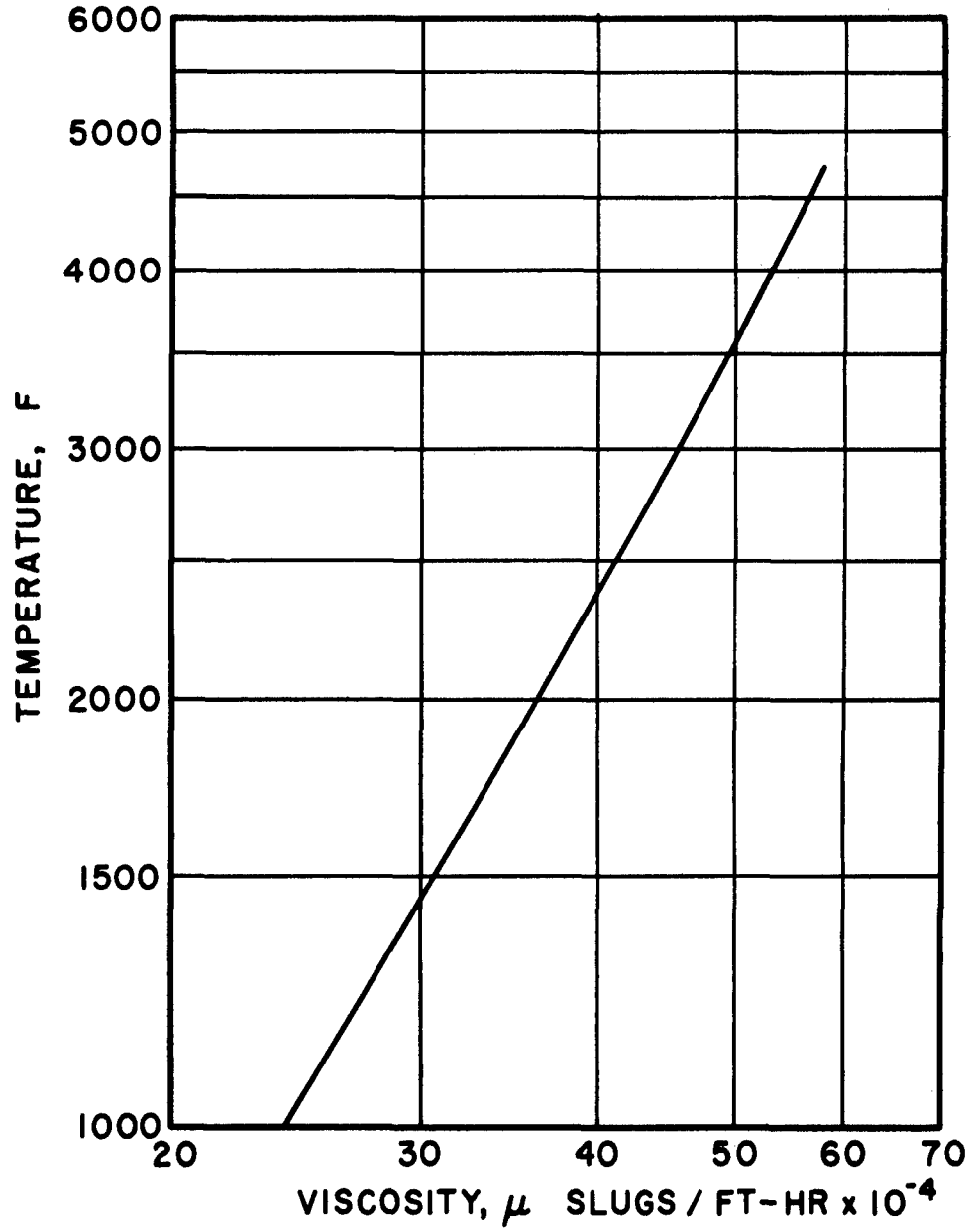

FIG. 21 ,VARIATION OF VISCOSITY OF COMBUSTION PRODUCTS OF NH_3-WFNA WITH TEMPERATURE, MIXTURE RATIO 1.4 TO 3.0

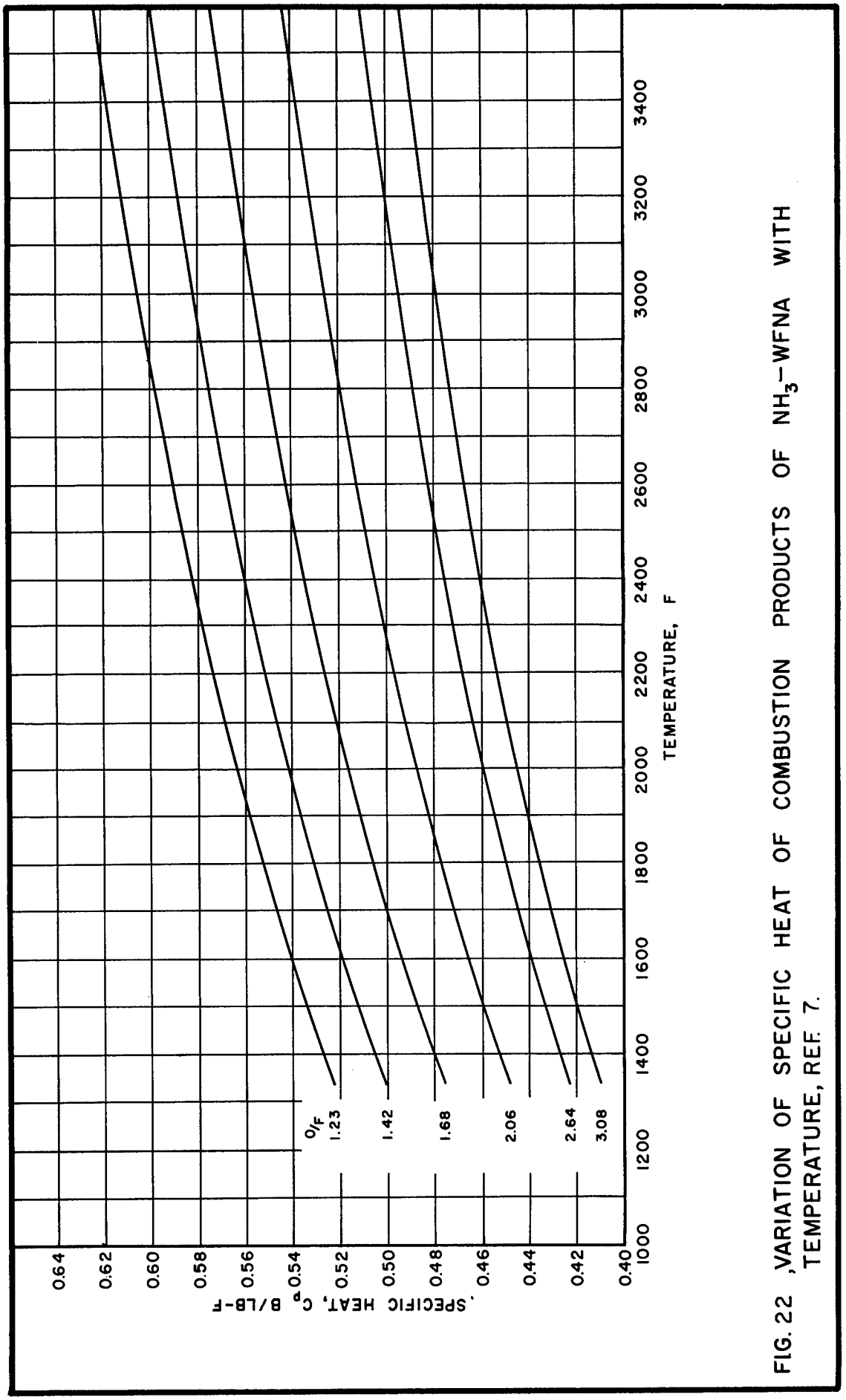

FIG. 22 ,VARIATION OF SPECIFIC HEAT OF COMBUSTION PRODUCTS OF NH_3-WFNA WITH TEMPERATURE, REF. 7.

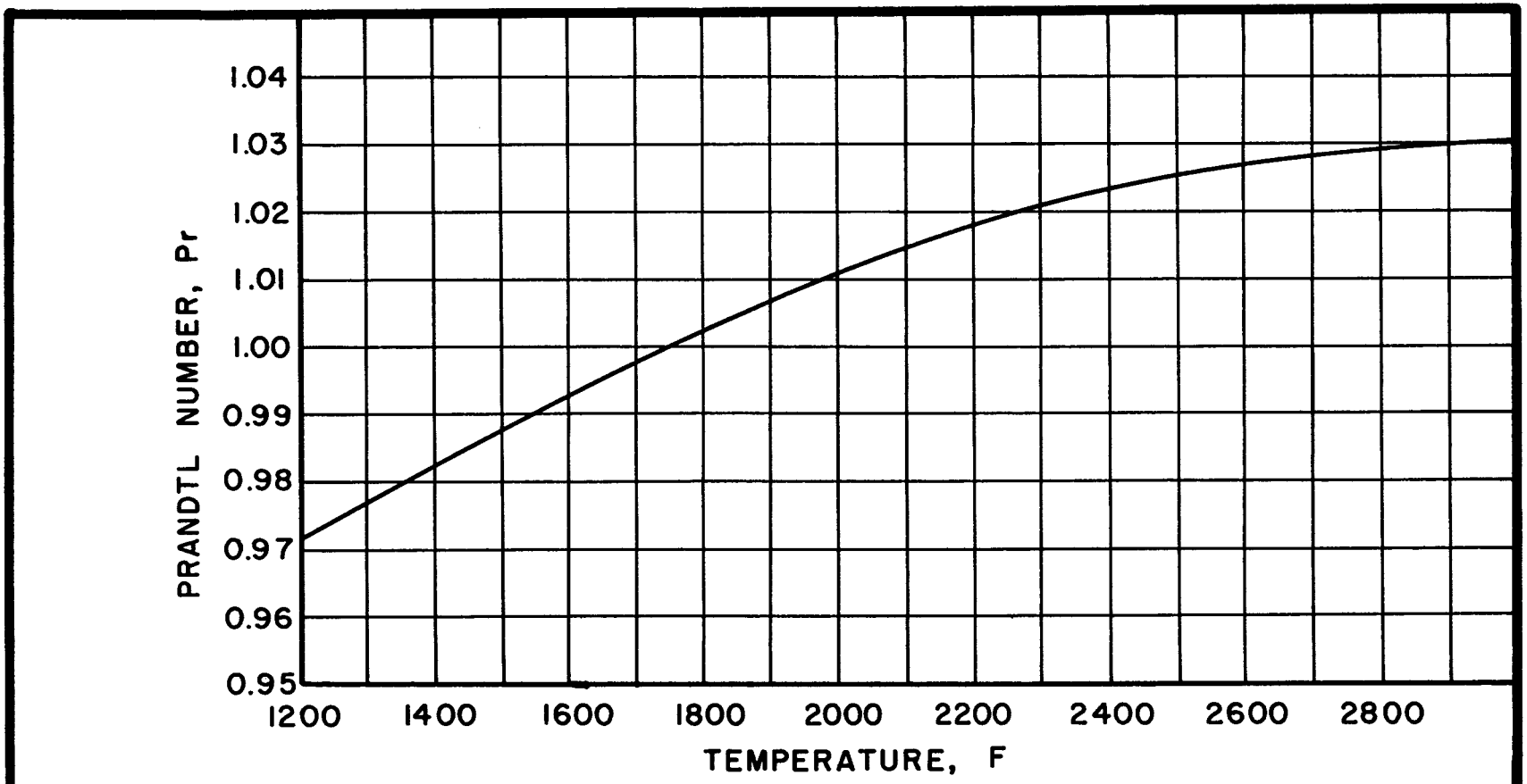

FIG. 23 ,VARIATION OF PRANDTL NUMBER OF COMBUSTION PRODUCTS OF NH_3–WFNA WITH TEMPERATURE, MIXTURE RATIOS 1.4 TO 3.0

As the heat transfer coefficient is based on the adiabatic wall temperature* and not the free stream static temperature, knowledge of the static temperature is not required for the evaluation of the film coefficient, h_g. However, in evaluating the physical properties, viscosity, thermal conductivity, and specific heat, some reference temperature must be chosen. For the data and calculations reported herein, all of the physical properties were evaluated at the arithmetic average of the wall and gas static temperature.

---

* The adiabatic wall temperature is that temperature the wall would assume if it were insulated.

APPENDIX 3

EXPERIMENTAL DATA

Heat Transfer

Calculation of Experimental Gas Film Coefficient

The methods employed by different investigators for determining local heat transfer coefficients in a converging-diverging nozzle are reviewed in the literature survey (5)(8)(9)(11)(17)(19). The method adopted in this program permitted the measurement of the local heat flux and coolant bulk temperature in and out of a nozzle test section. It was not possible in the adopted method to measure the temperature of the wall of the nozzle or the gas total temperature.

To compute local values of the gas film coefficient from measurements of the local heat flux, a thermal circuit with overall resistance, Ω_T, is considered. The overall resistance is related to the heat flux through the relation

$$\Omega_T = \frac{T_{aw} - T_{BL}}{q''} \qquad (3.1)$$

where q'' includes both the radiant and convective heat flux. The measurable quantities of equation 3.1 are the heat flux, q'', and the liquid bulk temperature T_{BL}, which is the average of the temperature of the liquid entering and leaving the section.

Since the coolant flow rate and temperature rise are known for each nozzle section, the heat flux may be obtained from the relation

$$q'' = \frac{\dot{W} c_p \Delta T}{A_s} \tag{3.2}$$

where A_s is the gas side heat transfer surface area.

The adiabatic wall temperature calculated from the expression

$$T_{aw} = T_\infty + \alpha (T_T - T_\infty) \tag{3.3}$$

where the recovery factor, α, is given by

$$\alpha = \sqrt[3]{Pr} \tag{3.4}$$

was assumed to be the <u>total temperature</u> as the Prandtl number was between 0.97 and 1.03 over the range of run conditions encountered.

The total temperature was calculated from experimentally determined values of the characteristic exhaust velocity, C*, and the value of the combustion chamber total temperature calculated by thermochemical methods. According to reference 26, for a nozzle discharge coefficient of unity, the characteristic exhaust velocity is given by the equation

$$C^* = \frac{223.0 \sqrt{\frac{T_c}{mw}}}{\sqrt{\gamma} \left(\frac{2}{\gamma + 1}\right)^{\frac{\gamma + 1}{2(\gamma - 1)}}} \tag{3.5}$$

It was assumed that variations in C* from theoretical values, based on thermochemical calculations, could be attributed to variations in the

combustion temperature. Hence, the gas total temperature, neglecting heat transfer losses, could be calculated from the relation

$$T_T = \left[\frac{C^*}{C^*_{Th}}\right]^2 T_{c_{Th}} \tag{3.6}$$

The determination of the actual characteristic exhaust velocity depends only on experimental determination of the combustion pressure, propellant flow rates, and nozzle throat diameter. The actual total temperature, computed from equation 3.6 was, on the average 88 per cent of the theoretical frozen equilibrium values of reference 7.

To calculate the gas film resistance it is necessary to resolve the total resistance into its component resistances. The total heat flux is the sum of the radiant and convective heat fluxes. Hence, the total resistance, Ω_T, consists of a convective gas film resistance in parallel with a radiation resistance both of which are in series with the wall and liquid film resistances, or

$$\Omega_T = \frac{\Omega_g \Omega_r}{\Omega_g + \Omega_r} + \Omega_w + \Omega_L \tag{3.7}$$

The quantities appearing in equation 3.7 are defined by the equations

$$\Omega_g = \frac{1}{h_g} \tag{3.8}$$

$$\Omega_w = \frac{d}{k_w} \tag{3.9}$$

$$\Omega_L = \frac{1}{h_L} \tag{3.10}$$

$$\Omega_r = \frac{T_{aw} - T_{wg}}{q_r''} \tag{3.11}$$

As the wall and liquid film resistances are both functions of temperature, it is necessary to calculate the gas and coolant side wall temperatures. The gas side wall temperature may be determined from the relation

$$T_{wg} = T_{aw} - q'' \left[\frac{\Omega_g \Omega_r}{\Omega_g + \Omega_r} \right] \tag{3.12}$$

or

$$T_{wg} = T_{aw} - (q'' - q_r'') \Omega_g \tag{3.13}$$

and the coolant side wall temperature may be computed from the equation

$$T_{wL} = T_{aw} - q'' \left[\frac{\Omega_g \Omega_r}{\Omega_g + \Omega_r} + \Omega_w \right] \tag{3.14}$$

As the wall thermal conductivity was evaluated at the average temperature $T_{wg} + T_{wL}/2$ and the physical properties appearing in the liquid film resistance were evaluated at the average temperature $T_{wL} + T_{BL}/2$, an iterative process was necessary to calculate the combination of the gas film and radiation resistances. A value for Ω_w and Ω_L was assumed and

$\Omega_g \Omega_r / \Omega_g + \Omega_r$ was calculated; using these calculated and assumed resistances, the wall temperatures T_{wg} and T_{wL} were computed from equations 3.12 and 3.14. With these wall temperatures known, the average wall temperature and the average liquid film temperature could be calculated. The wall thermal conductivity was then determined for the average wall temperature and the wall resistance to heat flow was calculated from equation 3.9. The liquid film resistance was evaluated at the average liquid film temperature (as explained in the next paragraph). Using these second approximations for the wall and liquid film resistances the iterative process was repeated until the assumed and calculated values were matched.

To facilitate data reduction, a generalized curve for the liquid film resistance was plotted. Kreith and Summerfield (14) recommend that for high heat flux densities the conventional Colburn equation for heat transfer in smooth tubes be used. The physical properties μ, ρ, k, and c_p are evaluated at the average film temperature. The Colburn equation is

$$Nu_D = 0.023 \, Re_D^{0.8} \, Pr^{1/3} \tag{3.15}$$

which can be rearranged in the form:

$$\frac{\Omega'_L \, V_L^{4/5}}{m^{1/5}} = \frac{0.023 \, \mu^{0.8}}{\rho^{0.8} \, k \, Pr^{1/3}} \tag{3.16}$$

The right hand side of equation 3.16 is a function only of temperature so that a curve of $\Omega'_L \, V_L^{4/5} / m^{1/5}$ may be plotted as a function of wall

temperature for a fixed value of liquid bulk temperature. A correction factor, C_H, is introduced to account for the coolant passage curvature. Hence, the liquid film resistance can be calculated from the equation

$$\Omega_L = \Omega_L' \frac{V_L^{4/5}}{m^{1/5}} \left[\frac{m^{1/5}}{C_H V_L^{4/5}} \right] \qquad (3.17)$$

McAdams (16) recommends the following correction for curvature

$$C_H = 1 + \frac{14m}{D_H} \qquad (3.18)$$

where m is the coolant passage hydraulic radius and D_H is the helix diameter of the coolant passage. Since the coolant velocity was nearly a constant throughout all of the runs, the bracketed term of equation 3.17 was assumed constant for a particular nozzle test section. Figure 24 shows the liquid film resistance parameter as a function of wall temperature for a coolant bulk temperature of 70 F.

In summary, the calculation procedure for the reduction of the gas film and radiation resistances is as follows:

1) Calculate the total resistance, Ω_T, employing equation 3.1,
2) Assume a value for Ω_w and Ω_L and calculate the resistance $\Omega_g\Omega_r/\Omega_g + \Omega_r$ using equation 3.7,
3) Compute the gas side and coolant side wall temperatures from equations 3.12 and 3.14,
4) Evaluate the wall thermal conductivity from Fig. 25 at the average wall temperature and recalculate Ω_w by means of

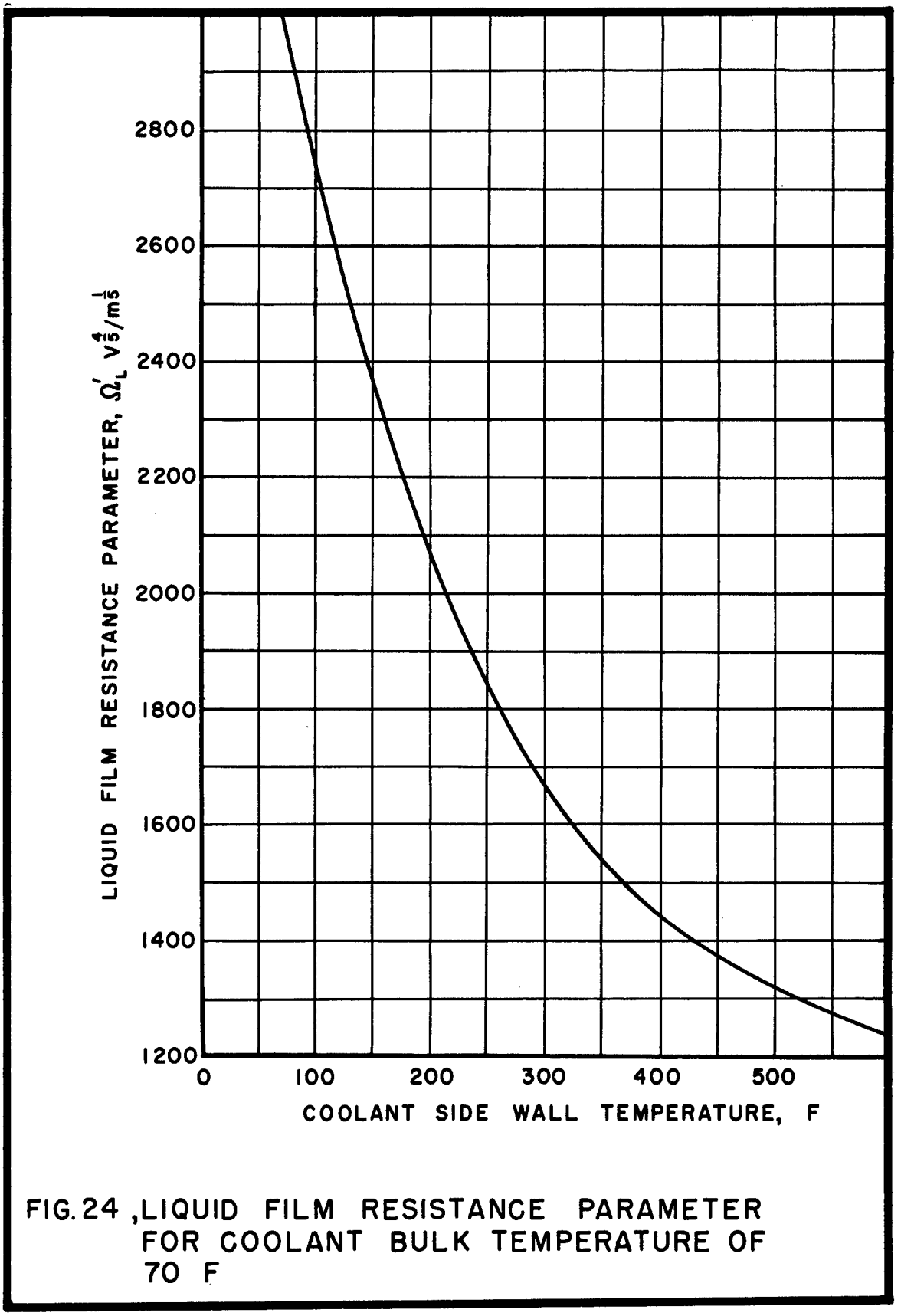

FIG. 24 ,LIQUID FILM RESISTANCE PARAMETER FOR COOLANT BULK TEMPERATURE OF 70 F

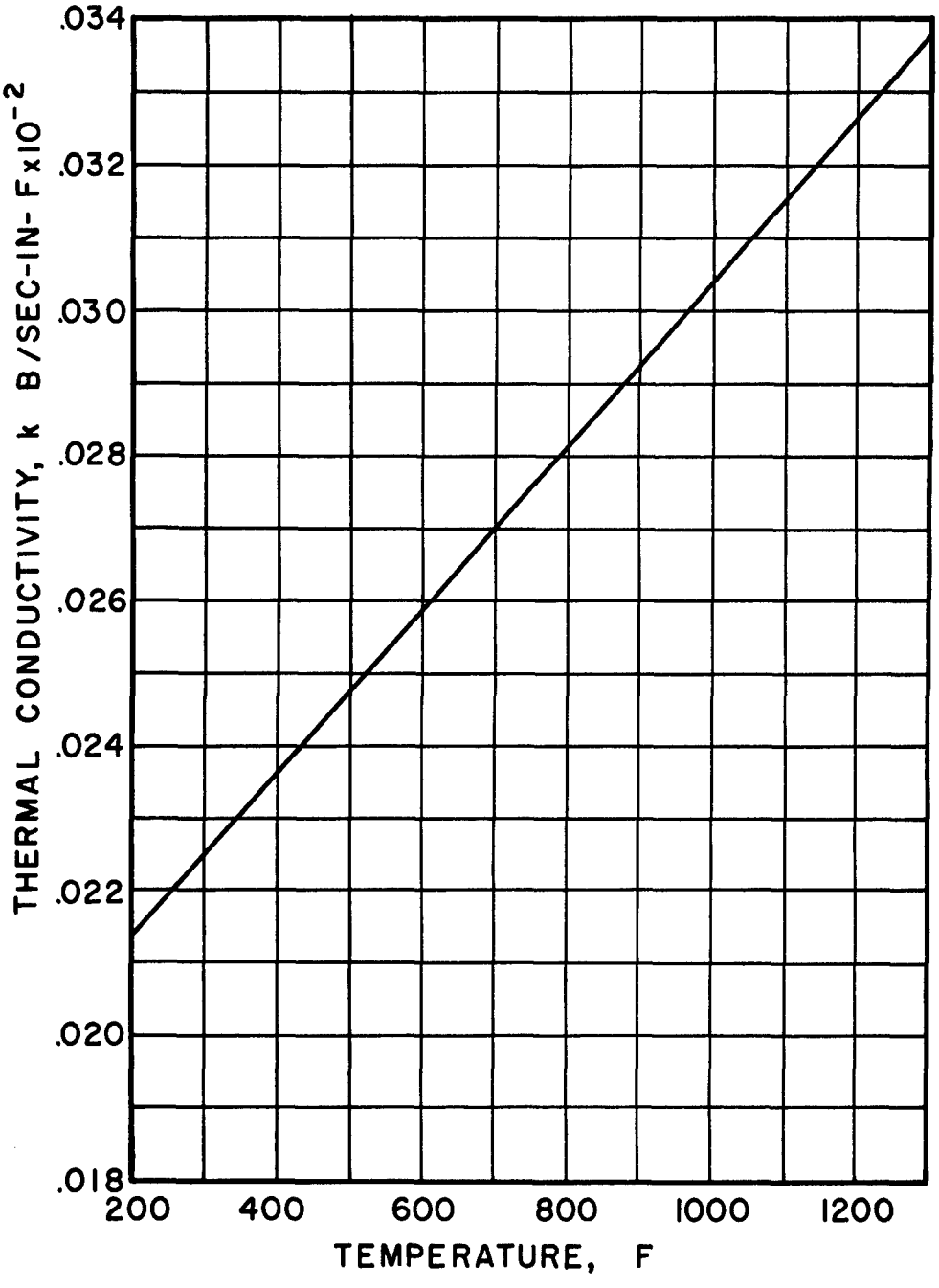

FIG. 25, VARIATION OF THERMAL CONDUCTIVITY OF TYPE 321 STAINLESS STEEL WITH TEMPERATURE, REF. 23.

equation 3.9. (The thermal conductivity of type 321 stainless steel was taken from reference 23),

5) Calculate the liquid film resistance employing Fig. 24 and equation 3.17 and

6) Recalculate the resistance $\Omega_g \Omega_r / \Omega_g + \Omega_r$ using equation 3.7.

Radiation Heat Flux

Employing the procedure previously described, the sum of the two parallel resistances Ω_r and Ω_g could be determined. To separate the radiation and convection resistances, an estimate of the radiant heat flux was made according to the method described in Appendix 5. It was assumed that radiation was constant throughout the combustion chamber and first three test sections. The computations indicated that in Sections 1, 2, and 3, convection accounts for an average of 85, 91, and 95 per cent of the total heat flux over a range of combustion pressures 500 to 1000 psia and mixture ratios from 1.4 to 3.0. According to the calculations, the radiant heat flux varied from a minimum of 0.10 Btu/sec in^2 at 500 psia combustion pressure and mixture ratio of 1.42 to a maximum of 0.34 Btu/sec in^2 at 999 psia combustion pressure and mixture ratio of 2.20.

It was believed that radiation in the throat (Section 4) and Sections 5 and 6 could be neglected. Due to the rapidly changing area ratio at the throat, the gas static temperature decreases and the convective film coefficient (sensitive to changes in the mass flow rate per unit area) rises quite sharply. In addition, the radiant heat flux is proportional to the area normal to the radiating gas in the combustion chamber and consequently

the convex throat surface would receive less radiation. For the aforementioned reasons, it seems reasonable that radiation could not account for more than 2 per cent of the throat heat flux. In the divergence cone, radiation is also greatly diminished due to the lower gas temperature.

To separate the convective and radiation heat fluxes it is noted that the total heat flux is given by

$$q'' = q_r'' + q_c'' \tag{3.19}$$

or

$$\frac{q_c''}{q''} = 1 - \frac{q_r''}{q''} \tag{3.20}$$

Therefore, the Nusselt number for convection could be calculated from the measured value of the combination of radiation and convection resistances, by the equation

$$Nu_D = \left[1 - \frac{q_r''}{q''}\right] \left[\frac{\Omega_r + \Omega_g}{\Omega_r \Omega_g}\right] \left[\frac{D}{k_{am}}\right] \tag{3.21}$$

The calculated radiant heat flux is presented in Fig. 27 (Appendix 5) as a function of mixture ratio for combustion pressures of 500 and 600 psia.

As indicated in Appendix 2, the physical properties appearing in the Nusselt, Reynolds, and Prandtl numbers were evaluated at the arithmetic mean film temperature.

Table 2 illustrates the procedure employed to calculate local values of the Nusselt number for convection from experimental measurements of the

heat flux. As indicated earlier, an iterative process was necessary; however, in Table 2, the iteration process was omitted and the correct values were assumed initially. The total resistance to heat flow, Ω_T, was computed from equation 3.1. For this run point, the adiabatic wall temperature (assumed to be the total temperature) computed from equation 3.6 was T_{aw} = 3900 F. The liquid bulk temperature was T_{BL} = 80 F.

The experimental heat flux for the combustion chamber and each nozzle section are given in Table 3. In addition, the calculated wall temperatures, Reynolds, Prandtl, and Nusselt numbers (corrected for radiation) are also presented. Nusselt numbers for the combustion chamber were not calculated.

Heat transfer results for Run 8 are omitted due to a failure of the thermocouple instrumentation system.

Table 2

Sample Calculation for Reduction of Heat Transfer Data

(Run Point 1 of Run 4)

Section	Ch	1	2	3	4	5	6	
$\dot{W}_{cool}$	1.026	0.353	0.202	0.223	0.524	0.351	0.351	lbs/sec
$\triangle t$	54.0	20.3	23.2	28.3	11.0	8.9	17.1	F
q	55.50	7.17	4.69	6.31	5.76	3.12	6.00	Btu/sec
A_s	35.29	4.364	2.010	1.304	0.986	1.235	2.416	in^2
q''	1.57	1.64	2.33	4.84	5.85	2.53	2.48	Btu/sec in^2
Ω_T	2433	2326	1638	789	653	1511	1537	sec in^2F/Btu
d	0.090	0.073	0.067	0.059	0.065	0.063	0.071	in
$T_{wg} + T_{wL}/2$	469	449	599	886	969	556	612	F
k_w	$0.0245(10)^{-2}$	0.0243	0.0259	0.0292	0.0301	0.0255	0.0261	Btu/sec in F
Ω_w	367	300	259	202	216	246	272	sec in^2F/Btu

Table 2 (Continued)

Section	Ch	1	2	3	4	5	6	
T_{wL}	179	200	278	363	329	249	273	F
$\cap'_I V_L^{4/5}/m^{1/5}$	2180	2070	1730	1470	1580	1840	1750	$\sec\frac{in^2}{Btu}$ $F(fps)^{4/5}/in^{1/5}$
$m^{1/5}/c_H V_L^{4/5}$	0.0288	0.0351	0.0491	0.0416	0.0260	0.038	0.0438	$in^{1/5}/(fps)^{4/5}$
$\cap_L$	63	73	85	61	41	70	77	sec in^2 F/Btu
$\cap_g \cap_r / \cap_g + \cap_r$	2003	1953	1294	526	396	1195	1188	sec in^2 F/Btu
T_{wg}	755	693	884	1355	1585	879	949	F
T_∞	—	3900	3883	3856	3447	2466	1938	F
T_{am}	—	2296	2383	2605	2516	1672	1493	F
T_∞ / T_{am}	—	1.585	1.522	1.410	1.315	1.371	1.229	—
μ_{am}	—	$39.1(10)^{-4}$	40.1	42.1	41.3	32.7	30.6	slug/ft hr

Table 2 (Continued)

Section	Ch	1	2	3	4	5	6	
D	—	2.002	1.390	0.904	0.612	0.827	1.127	in
Re_D	—	$3.39(10)^5$	4.56	6.20	8.70	8.50	5.95	———
Pr	—	1.014	1.017	1.023	1.026	0.984	0.972	———
k_{am}	—	0.059	0.0602	0.0641	0.0628	0.0471	0.0438	Btu/hr ft F
Nu_{Du}	—	750	771	1155	1065	635	935	———
$q_r^{''}$	—	0.21	0.21	0.21	———	———	———	Btu/sec in^2
Nu_D	—	653	702	1105	1065	635	935	———

Table 3

Summary of Experimental Heat Transfer Data

Run 4

Section	Ch	1	2	3	4	5	6
q''	1.57	1.64	2.33	4.84	5.85	2.53	2.48
T_{wg}	755	693	884	1355	1585	879	949
Nu_D	____	653	702	1105	1065	635	935
Re_d	____	$3.39(10)^5$	4.56	6.20	8.70	8.50	5.95
Pr	____	1.014	1.017	1.023	1.026	0.984	0.972
q''	1.36	1.47	2.26	4.53	5.88	2.72	2.32
T_{wg}	681	641	868	1312	1615	930	895
Nu_D	____	623	732	1105	1184	743	959
Re_D	____	$3.55(10)^5$	4.76	6.36	8.84	8.46	6.55
Pr	____	1.018	1.021	1.026	1.025	0.995	0.981
q''	1.43	1.67	2.51	4.78	6.45	2.87	2.44
T_{wg}	706	734	978	1406	1788	1034	976
Nu_d	____	713	811	1150	1305	721	933
Re_D	____	$3.78(10)^5$	4.99	6.75	9.18	7.83	6.06
Pr	____	1.027	1.028	1.030	1.030	1.019	1.008

Point	O/F	P_c	T_{aw}	q''_r
1	2.42	506	3900	0.21
2	2.63	502	3730	0.20
3	2.24	500	3930	0.22

Note: Temperatures have the units-F. Heat fluxes have the units - Btu/sec in^2. Combustion pressures have the units - psia.

Table 3 (Continued)

Run 5

Section	Ch	1	2	3	4	5	6
q''	1.30	1.38	2.15	4.22	6.35	2.78	2.24
T_{wg}	657	620	838	1231	1683	940	880
Nu_D	____	642	724	962	1410	806	984
Re_D	____	$3.06(10)^5$	4.54	6.20	8.07	7.99	6.20
Pr	____	1.020	1.019	1.024	1.025	0.993	0.979
q''	1.29	1.50	2.35	4.31	6.61	2.90	2.34
T_{wg}	659	653	903	1246	1729	960	917
Nu_D	____	723	873	1178	1621	895	1094
Re_D	____	$3.42(10)^5$	4.52	6.28	8.46	8.01	6.20
Pr	____	1.018	1.022	1.024	1.025	1.003	0.982
q''	1.28	1.48	2.33	3.96	6.51	2.89	2.26
T_{wg}	646	638	880	1189	1721	971	882
Nu_D	____	715	857	1060	1610	895	1052
Re_D	____	$3.51(10)^5$	4.68	6.52	8.23	8.20	6.46
Pr	____	1.015	1.017	1.024	1.025	0.994	0.978
q''	1.28	1.43	2.14	3.54	5.75	2.88	2.11
T_{wg}	659	630	837	1096	1582	972	848
Nu_D	____	780	885	1045	1555	992	1097
Re_D	____	$3.67(10)^5$	4.93	6.97	8.80	8.45	6.87
Pr	____	1.011	1.015	1.022	1.024	0.997	0.978

Point	O/F	P_c	T_{aw}	q_r''
1	2.22	476	3620	0.21
2	1.97	486	3500	0.19
3	1.80	491	3375	0.17
4	1.59	492	3135	0.14

Table 3 (Continued)

Run 6

Section	Ch	1	2	3	4	5	6
q''	1.54	1.55	2.48	4.13	5.52	2.48	2.43
T_{wg}	745	664	920	1227	1528	848	931
Nu_D	____	585	723	870	969	597	889
Re_D	____	$3.45(10)^5$	4.59	6.51	8.90	8.75	6.41
Pr	____	1.022	1.025	1.027	1.027	0.997	0.986
q''	1.39	1.43	2.29	3.87	5.42	2.35	2.32
T_{wg}	692	628	774	1150	1511	850	906
Nu_D	____	581	713	872	1007	587	926
Re_D	____	$3.62(10)^5$	4.88	6.83	9.31	8.87	6.70
Pr	____	1.019	1.024	1.025	1.024	0.998	0.982
q''	1.28	1.37	2.16	3.24	4.67	1.96	2.01
T_{wg}	651	608	794	1015	1370	740	885
Nu_D	____	659	794	833	1000	589	932
Re_D	____	$3.83(10)^5$	5.16	7.40	10.0	9.91	7.05
Pr	____	1.013	1.017	1.020	1.019	0.983	0.976

Point	O/F	P_c	T_{aw}	q_r''
1	2.53	524	3990	0.21
2	2.75	519	3820	0.19
3	2.92	509	3500	0.17

Table 3 (Continued)

Run 7

Section	Ch	1	2	3	4	5	6
q''	1.49	1.74	2.48	4.07	7.15	3.23	2.34
T_{wg}	685	680	890	1188	1797	987	872
Nu_D	____	732	802	945	1542	886	963
Re_D	____	$3.28(10)^5$	4.44	6.08	7.91	7.87	6.24
Pr	____	1.020	1.022	1.026	1.027	0.998	0.981
q''	1.46	1.69	2.36	3.62	6.78	3.15	2.31
T_{wg}	714	707	895	1107	1758	1047	896
Nu_D	____	797	841	888	1568	929	1010
Re_D	____	$2.88(10)^5$	4.72	5.34	8.20	10.9	6.40
Pr	____	1.014	1.016	1.023	1.024	0.993	0.977
q''	1.23	1.46	1.93	2.88	5.66	2.68	1.94
T_{wg}	632	637	766	931	1538	925	782
Nu_D	____	889	864	888	1456	1007	1084
Re_D	____	$3.80(10)^5$	5.19	7.55	9.06	8.83	7.12
Pr	____	1.002	1.004	1.007	1.013	0.981	0.964

Point	O/F	P_c	T_{aw}	q_r''
1	2.06	495	3800	0.21
2	1.74	507	3460	0.16
3	1.42	501	2930	0.10

Table 3 (Continued)

Run 9

Section	Ch	1	2	3	4	5	6
q''	1.21	1.29	2.21	4.16	7.94	4.33	2.60
T_{wg}	620	579	850	1212	1959	1292	977
Nu_D	____	465	638	903	1622	1145	1000
Re_D	____	$4.01(10)^5$	5.35	7.42	9.07	8.35	7.15
Pr	____	1.020	1.023	1.026	1.028	1.006	0.986
q''	1.10	0.99	1.88	4.03	6.78	4.13	2.44
T_{wg}	577	480	762	1204	1791	1261	938
Nu_D	____	341	537	879	1318	1096	946
Re_D	____	$4.46(10)^5$	5.88	6.57	10.2	9.02	7.75
Pr	____	1.018	1.022	1.026	1.027	1.005	0.984
q''	0.97	1.01	1.80	3.77	6.43	3.73	2.21
T_{wg}	526	483	729	1138	1707	1172	873
Nu_D	____	417	598	955	1477	1148	987
Re_D	____	$4.81(10)^5$	6.41	8.67	11.0	9.92	8.56
Pr	____	1.012	1.017	1.022	1.025	0.998	0.978

Point	O/F	P_c	T_{aw}	q_r''
1	2.11	601	3920	0.25
2	2.68	621	3900	0.22
3	2.97	626	3585	0.20

Table 3 (Continued)

Run 10

Section	Ch	1	2	3	4	5	6
q''	1.11	1.31	2.05	4.55	8.17	4.31	2.51
T_{wg}	583	588	805	1298	2014	1291	953
Nu_D	____	487	598	1036	1772	1176	989
Re_D	____	$4.15(10)^5$	5.61	7.47	9.24	8.61	7.42
Pr	____	1.019	1.016	1.027	1.029	1.006	0.984
q''	1.08	1.22	2.00	4.24	7.58	4.10	2.47
T_{wg}	568	557	793	1246	1918	1255	947
Nu_D	____	452	570	909	1528	1064	931
Re_D	____	$4.16(10)^5$	5.59	7.53	9.34	8.65	7.36
Pr	____	1.017	1.021	1.025	1.027	1.003	0.983
q''	0.98	1.05	1.79	4.14	6.35	3.81	2.36
T_{wg}	532	500	730	1221	1687	1184	911
Nu_D	____	448	588	1030	1404	1137	1018
Re_D	____	$4.45(10)^5$	5.94	7.82	10.1	9.11	7.70
Pr	____	1.010	1.014	1.021	1.023	0.996	0.977
q''	0.92	1.33	2.20	4.58	7.58	4.46	2.69
T_{wg}	507	593	847	1311	1901	1326	1003
Nu_D	____	477	627	1007	1493	1172	1023
Re_D	____	$4.11(10)^5$	5.49	7.43	9.47	8.49	7.50
Pr	____	1.020	1.023	1.027	1.028	1.007	0.986

Point	O/F	P_c	T_{aw}	q_r''
1	2.17	612	3860	0.25
2	1.75	623	3760	0.18
3	1.53	624	3440	0.14
4	2.20	616	3940	0.26

Table 3 (Continued)

Run 11

Section	Ch	1	2	3	4	5	6
q''	1.22	1.32	2.21	3.77	5.77	3.79	2.26
T_{wg}	626	593	713	1157	1622	1189	891
Nu_D	____	555	725	940	1244	1136	968
Re_D	____	$4.01(10)^5$	5.75	7.72	10.1	8.76	7.56
Pr	____	1.015	1.017	1.023	1.024	1.00	0.979
q''	1.37	1.38	2.29	3.81	5.77	3.97	2.33
T_{wg}	678	602	866	1157	1584	1218	907
Nu_D	____	624	800	954	1149	1205	1032
Re_D	____	$4.39(10)^5$	5.49	8.00	10.4	8.89	7.71
Pr	____	1.005	1.010	1.016	1.023	0.992	0.972
q''	1.25	1.26	1.90	3.11	4.49	3.48	2.13
T_{wg}	636	573	773	981	1333	1093	843
Nu_D	____	676	737	880	1080	1231	1093
Re_D	____	$4.64(10)^5$	6.16	8.89	11.8	9.96	8.33
Pr	____	1.004	1.008	1.012	1.012	0.988	0.969
q''	1.19	1.30	2.15	3.64	5.85	3.94	2.28
T_{wg}	615	584	835	1098	1585	1203	887
Nu_D	____	485	631	778	1070	1039	880
Re_D	____	$4.05(10)^5$	5.39	7.69	10.1	9.95	7.45
Pr	____	1.019	1.023	1.025	1.026	1.004	0.983

Point	O/F	P_c	T_{aw}	q_r''
1	1.97	595	3630	0.23
2	1.67	622	3580	0.17
3	1.40	627	3540	0.12
4	1.97	608	3890	0.23

Table 3 (Continued)

Run 12

Section	Ch	1	2	3	4	5	6
q''	1.46	1.51	2.57	3.87	6.30	3.10	2.13
T_{wg}	712	649	955	1153	1683	1022	846
Nu_D	____	608	820	875	1248	825	855
Re_D	____	$3.82(10)^5$	5.02	4.81	9.46	8.94	7.30
Pr	____	1.019	1.023	1.025	1.026	0.998	0.981
q''	1.54	1.64	2.94	4.38	7.30	3.64	2.32
T_{wg}	745	694	1048	1254	1858	1143	899
Nu_D	____	696	1010	1060	1624	1037	963
Re_D	____	$3.96(10)^5$	5.14	7.45	9.38	8.97	7.45
Pr	____	1.018	1.023	1.025	1.027	1.000	0.981
q''	1.50	1.59	2.72	3.93	6.54	3.47	2.24
T_{wg}	731	681	990	1184	1733	1102	881
Nu_D	____	690	917	936	1395	981	937
Re_D	____	$4.23(10)^5$	5.36	7.81	9.99	9.28	7.74
Pr	____	1.016	1.023	1.024	1.026	0.999	0.980
q''	1.35	1.51	2.53	3.52	5.90	3.21	2.02
T_{wg}	677	650	944	1093	1610	1049	822
Nu_D	____	682	907	887	1322	950	894
Re_D	____	$4.28(10)^5$	5.63	8.31	10.6	9.81	8.11
Pr	____	1.015	1.020	1.021	1.023	0.995	0.977

Point	O/F	P_c	T_{aw}	q''_r
1	2.37	562	3800	0.23
2	2.21	586	3720	0.24
3	2.38	596	3715	0.23
4	2.61	595	3575	0.22

Table 3 (Continued)

Run 13

Section	Ch	1	2	3	4	5	6
q''	1.71	1.63	2.83	4.43	6.70	3.82	2.58
T_{wg}	804	691	1019	1278	1758	1183	969
Nu_D	____	665	923	1057	1387	1071	1050
Re_D	____	$4.31(10)^5$	5.81	8.06	10.5	9.70	9.08
Pr	____	1.019	1.024	1.026	1.027	1.002	0.983
q''	1.71	1.87	3.07	4.59	7.25	4.15	2.50
T_{wg}	807	761	1074	1308	1855	1252	952
Nu_D	____	770	1010	1088	1534	1166	1020
Re_D	____	$4.57(10)^5$	5.98	8.67	11.1	10.1	8.59
Pr	____	1.021	1.025	1.026	1.027	1.004	0.983
q''	1.77	2.02	3.21	4.63	7.83	4.31	2.67
T_{wg}	828	805	1111	1318	1928	1285	1002
Nu_D	____	810	1010	1048	1853	1162	1041
Re_D	____	$4.74(10)^5$	6.28	9.11	11.5	10.6	8.91
Pr	____	1.023	1.026	1.027	1.018	1.006	0.986
q''	1.78	2.13	3.31	4.59	7.84	4.40	2.74
T_{wg}	832	861	1141	1318	1934	1310	1014
Nu_D	____	827	1100	1092	1724	1253	1119
Re_D	____	$5.02(10)^5$	6.66	9.77	12.3	11.7	9.46
Pr	____	1.022	1.026	1.026	1.028	1.005	0.985

Point	O/F	P_c	T_{aw}	q_r''
1	2.16	647	3781	0.26
2	2.23	698	3800	0.28
3	2.17	752	3888	0.29
4	2.21	793	3792	0.31

Table 3 (Continued)

Run 14

Section	Ch	1	2	3	4	5	6
q''	1.69	1.79	2.60	3.79	6.51	3.87	2.54
T_{wg}	801	743	969	1083	1725	1201	966
Nu_D	____	793	897	943	1487	1187	1136
Re_D	____	$5.30(10)^5$	7.12	10.6	13.1	11.8	9.72
Pr	____	1.017	1.021	1.022	1.025	0.999	0.981
q''	1.99	2.24	3.16	4.39	7.69	4.32	2.76
T_{wg}	900	872	1098	1276	1810	1367	1020
Nu_D	____	982	1061	1065	1983	1279	976
Re_D	____	$5.67(10)^5$	7.64	11.2	12.9	11.0	8.16
Pr	____	1.021	1.024	1.026	1.029	1.006	1.004
q''	2.14	2.38	3.38	4.59	7.67	4.62	3.03
T_{wg}	947	911	1157	1312	1882	1347	1082
Nu_D	____	1018	1115	1085	1646	1309	1253
Re_D	____	$6.26(10)^5$	8.35	12.3	15.8	13.9	11.6
Pr	____	1.023	1.025	1.026	1.028	1.006	0.986

Point	O/F	P_c	T_{aw}	q_r''
1	2.22	774	3600	0.30
2	2.20	885	3730	0.33
3	2.20	999	3800	0.34

Performance

The experimental performance data tabulated in Table 4 were calculated from the following equations (26):

$$I_{sp} = \frac{F}{\dot{w}_p} \tag{3.22}$$

$$C^* = \frac{A^* P_c g}{\dot{w}_p} \tag{3.23}$$

$$C_F = \frac{F}{A^* P_c} \tag{3.24}$$

Specific Impulse Correction

Values of the specific impulse corrected for heat transfer are also presented. A heat transfer correction for the specific impulse is necessary when data obtained with a low thrust motor are to be applied to a high thrust motor. In the latter case, the amount of heat transferred per pound of propellant is much less due to the smaller surface to volume ratio.

There are two types of heat transfer corrections: an adiabatic correction and a regenerative correction. In both corrections it is assumed that the heat transferred to the coolant water in the experimental motor could have been utilized to increase the jet kinetic energy of the exhaust gases. As not all of the heat lost to the coolant water can be converted to jet kinetic energy some efficiency of energy conversion must be chosen.

In the regenerative correction that efficiency is

$$e = 1 - \left[\frac{P_a}{P_c}\right]^{\frac{\gamma - 1}{\gamma}} \qquad (3.25)$$

For the adiabatic correction the efficiency is of the same form as equation 3.25 except that the local pressure at which each unit of heat was transferred is substituted for the combustion pressure, P_c. It is apparent that the regenerative correction is always higher than the adiabatic correction. The correction reported herein is the regenerative correction. The corrected specific impulse is the specific impulse that would be obtained if the experimental motor were regeneratively cooled. The derivation of the specific impulse correction is given below.

According to reference 18, an energy balance on one pound of combustion gas gives:

$$\frac{V_{ec}^2}{2gJ} = \frac{V_e^2}{2gJ} + \frac{eq}{\dot{w}_p} \qquad (3.26)$$

or

$$V_{ec}^2 = V_e^2 + \frac{2gJ\,eq}{\dot{w}_p} \qquad (3.27)$$

Using the relations:

$$I_{sp} = \frac{V_e}{g} \qquad (3.28)$$

$$I'_{spc} = \frac{V_{ec}}{g} \qquad (3.29)$$

The specific impulse, corrected for heat transfer, becomes

$$I'_{spc} = \sqrt{I_{sp}^2 + \frac{2Je}{g}\frac{q}{w_p}} \qquad (3.30)$$

It was not possible to operate the motor exactly at the selected value of chamber pressure. Consequently, it was necessary to make a correction for experimental deviations in the chamber pressure from the nominally selected run conditions. From the thermodynamic relation (26)

$$I_{sp} = 6.93\,\lambda\,\phi\sqrt{\frac{T_c}{mw}}\sqrt{\frac{2\gamma}{\gamma-1}}\sqrt{1-\left[\frac{P_a}{P_c}\right]^{\frac{\gamma-1}{\gamma}}} \qquad (3.31)$$

it is seen that for constant λ, ϕ, γ, and $\frac{T_c}{mw}$ the chamber pressure correction is given by

$$\frac{\sqrt{1-\left[\frac{P_a}{P_{cn}}\right]^{\frac{\gamma-1}{\gamma}}}}{\sqrt{1-\left[\frac{P_a}{P_c}\right]^{\frac{\gamma-1}{\gamma}}}}$$

Substituting equation 3.25 into the above ratio gives the following expression for the pressure correction:

$$\frac{\sqrt{1-\left[\frac{P_a}{P_{cn}}\right]^{\frac{\gamma-1}{\gamma}}}}{\sqrt{e}}$$

where P_{cn} is the nominally chosen chamber pressure (either 500 or 600 psia). Hence, the corrected value of the specific impulse is the product of the chamber pressure and heat transfer corrections, or

$$I_{spc} = \sqrt{\frac{1 - \left[\frac{P_a}{P_{cn}}\right]^{\frac{\gamma - 1}{\gamma}}}{e}} \sqrt{I_{sp}^2 + \frac{2Je}{g}\frac{q}{\dot{w}_p}} \qquad (3.32)$$

which can be rearranged in the ratio form

$$\frac{I_{spc}}{I_{sp}} = \sqrt{\frac{1 - \left[\frac{P_a}{P_{cn}}\right]^{\frac{\gamma - 1}{\gamma}}}{e}} \sqrt{1 + \frac{2Je}{gI_{sp}^2}\frac{q}{\dot{w}_p}} \qquad (3.33)$$

To illustrate the relative magnitutde of the specific impulse correction, the first run point of run 4* is chosen as an example. The data are

$O/F = 2.42$

$P_c = 506$ psia

$P_a = 14.4$ psia

$F = 214$ lbs

$\dot{w}_p = 0.980$ lbs/sec

$q = 88.45$ Btu/sec (sum of local values from Table 2)

---

* As previously noted the mixture ratio was varied during each run. The results at each mixture ratio is called a run point. Thus a run consists of three or four run points.

$$\gamma = 1.213, \text{ (reference 7)}$$

From equation 3.22, the experimental specific impulse is

$$I_{sp} = \frac{214}{0.980} = 218.4 \text{ sec}$$

From equation 3.25,

$$e = 1 - \left[\frac{14.4}{506}\right]^{\frac{0.213}{1.213}} = 0.465$$

Using equation 3.33, the ratio of the corrected to the measured specific impulse is

$$\frac{I_{spc}}{I_{sp}} = \sqrt{\frac{1 - \left[\frac{14.4}{506}\right]^{\frac{0.213}{1.213}}}{0.465}} \sqrt{1 + \frac{2(778)(0.465)}{32.17(218.4)^2}\frac{88.45}{0.980}} = 1.021$$

Hence, the correction increases the experimentally determined value of specific impulse by 2.1 per cent. The corrected value is

$$I_{spc} = 1.021\ (218.4)$$

$$= 223 \text{ sec}$$

The experimentally determined values of combustion pressure, thrust, oxidizer and fuel flow rates and the performance parameters, calculated from equations 3.22, 3.23, 3.24, and 3.32 are tabulated in Table 4 for each run point.

Table 4

Tabulated Performance Data

Run No.	Run Duration min:sec	P_c psia	F lbs	$\dot{W}_{ox}$ lbs/sec	$\dot{W}_f$ lbs/sec	$\dot{W}_p$ lbs/sec	O/F
4	3:59	506	214	0.694	0.286	0.980	2.42
		502	211	0.724	0.276	1.000	2.63
		500	211	0.661	0.293	0.954	2.24
5	4:01	477	196	0.644	0.291	0.935	2.22
		486	202	0.626	0.219	0.945	1.97
		491	202	0.612	0.340	0.952	1.80
		492	202	0.591	0.372	0.963	1.59
6	4:00	524	220	0.716	0.284	1.000	2.53
		519	219	0.752	0.274	1.026	2.75
		509	215	0.785	0.265	1.050	2.92
7	3:32	495	207	0.635	0.308	0.943	2.06
		507	215	0.614	0.353	0.967	1.74
		501	210	0.583	0.411	0.994	1.42
8	3:22	578	239	0.763	0.358	1.121	2.13
		578	239	0.820	0.340	1.160	2.41
		580	240	0.866	0.332	1.198	2.61
9	4:05	601	250	0.769	0.364	1.133	2.11
		621	255	0.881	0.329	1.210	2.68
		626	256	0.952	0.321	1.273	2.97
10	4:00	612	257	0.799	0.368	1.167	2.17
		623	261	0.733	0.418	1.151	1.75
		624	261	0.709	0.462	1.171	1.53
		616	256	0.800	0.364	1.164	2.20
11	4:10	595	247	0.759	0.386	1.145	1.97
		622	260	0.727	0.436	1.163	1.67
		627	261	0.703	0.502	1.205	1.40
		608	253	0.754	0.383	1.137	1.97
12	3:56	562	235	0.766	0.323	1.089	2.37
		586	249	0.784	0.355	1.139	2.21
		596	253	0.823	0.346	1.169	2.38
		595	251	0.867	0.332	1.199	2.61
13	3:19	647	269	0.850	0.394	1.244	2.16
		698	294	0.930	0.417	1.347	2.23
		752	319	0.979	0.451	1.430	2.17
		793	337	1.050	0.475	1.525	2.21
14	3:40	774	329	1.054	0.475	1.529	2.22
		885	380	1.180	0.536	1.716	2.20
		999	433	1.322	0.602	1.924	2.20

Table 4 (Continued)

Run No.	C_F	C* fps	I_{sp} sec	I_{spc} sec	Comments
4	1.430	4917	218.4	223.0	Good run
	1.419	4778	211.0	213.7	
	1.425	4975	220.5	223.2	
5	1.410	4790	210.0	215.4	Rough combustion at low-
	1.420	4830	213.5	218.5	est mixture ratio
	1.406	4840	212.0	216.5	point
	1.408	4790	209.0	213.0	
6	1.430	4950	220.3	224.5	Good run
	1.435	4780	213.5	217.5	
	1.435	4580	202.5	206.5	
7	1.418	4970	219.5	223.5	Rough combustion at
	1.436	4930	222.0	226.5	second point
	1.428	4760	211.5	215.5	
8	1.410	4870	213.0	218.5	Shutdown for acid leak in
	1.410	4710	206.0	209.0	propellant cubicle
	1.410	4580	200.0	202.5	
9	1.410	5020	221.0	223.5	Good run
	1.396	4850	210.5	213.5	
	1.393	4640	201.0	204.0	
10	1.427	4960	220.0	223.5	Good run
	1.420	5090	226.2	229.0	
	1.420	5030	222.2	224.0	
	1.410	4990	220.0	222.5	
11	1.410	4910	216.0	218.0	Rough combustion at low-
	1.417	5040	223.5	227.5	est mixture ratio
	1.415	4920	216.3	218.0	
	1.417	5050	222.3	225.0	
12	1.420	4870	216.0	219.9	Repeat of Run 8.
	1.440	4860	219.0	222.4	Good run
	1.440	4817	216.3	219.9	
	1.440	4685	209.7	213.1	
13	1.416	4916	216.0	220.8	Good run
	1.434	4899	218.0	222.5	
	1.442	4968	223.0	226.8	
	1.447	4914	221.0	224.9	
14	1.450	4785	215.5	218.8	Good run
	1.460	4872	221.5	225.2	
	1.470	4905	225.0	228.6	

Note: Run 1 was checkout run for first sectional nozzle.
Runs 2 and 3 were checkout runs for second sectional nozzle.

APPENDIX 4

BIBLIOGRAPHY

1. Bartz, D. R., "An Approximate Solution of Compressible Turbulent Boundary-Layer Development and Convective Heat Transfer in Convergent-Divergent Nozzles", Progress Report No. 20-234, Jet Propulsion Laboratory, California Institute of Technology, 1954.

2. Bartz, D. R., "A Simple Equation for Rapid Estimation of Rocket Nozzle Convective Heat Transfer Coefficients", External Publication No. 351, Jet Propulsion Laboratory, California Institute of Technology, 1956.

3. Beighley, C. M. and Robison, D. E., "Testing and Design Procedures Employed in Research High Combustion Pressure Rocket Motors", Report No. RM-53-2, Purdue University Rocket Laboratory, April 1953.

4. Bird, R. B., Hirschfelder, J. O., and Curtiss, C. F., "Theoretical Calculation of the Equation of State and Transport Properties of Gases and Liquids", Transactions ASME, Vol. 76, Oct. 1954.

5. Boden, R. H., "Heat Transfer in Rocket Motors and the Application of Film and Sweat Cooling", Transactions ASME, Vol. 73, May 1951.

6. Brandes, D. J., "Determination of the Requirements for Film Cooling a 500 Pound Thrust Rocket Motor at 500 psia Combustion Pressure with White Fuming Nitric Acid", MS Thesis, Mechanical Engineering, Purdue University, June 1957.

7. Brinkley, S. R., Smith, R. W., Haben, M. A., and Edwards, H. E., "Thermodynamics of the Combustion Products of Ammonia with Nitric Acid", Bureau of Mines Report PX3-107/11, United States Department of the Interior, 1953.

BIBLIOGRAPHY (Continued)

8. Ellion, M. E., "New Techniques for Obtaining Heat Transfer Parameters of the Wall and Combustion Gas in a Rocket Motor", Transactions ASME, Vol. 73, Feb. 1951.

9. Gordon, R., "Heat Transfer Problems in Liquid Propellant Rocket Motors", Journal of the American Rocket Society, Vol. 81, June 1950.

10. Graham, A. R., "Film Cooling of Rocket Motors", Ph.D. Thesis, Mechanical Engineering, Purdue University, Jan. 1958.

11. Greenfield, S. "Determination of Rocket Motor Heat Transfer Coefficients by the Transient Method", Journal of the Aeronautical Sciences, Vol. 18, Aug. 1951.

12. Hilsenrath, J., et al, "Tables of Thermal Properties of Gases", National Bureau of Standards Circular 564, 1955.

13. Keenan, J. H. and Kaye, J., Gas Tables, John Wiley and Sons, Inc., 1948.

14. Kreith, F., and Summerfield, M., "Investigation of Heat Transfer at High Heat-Flux Densities: Experimental Study with Water of Friction-Drop and Forced Convection with and without Surface Boiling in Tubes", Progress Report No. 4-68, Jet Propulsion Laboratory, California Institute of Technology, 1948.

15. Leeds and Northrup Co., "Standard Conversion Tables for L&N Thermocouples", Standard 31031.

16. McAdams, W. H., "Heat Transmission, McGraw-Hill Book Co., Inc., 1954.

BIBLIOGRAPHY (Continued)

17. Ragsdale, W. C., "Heat Transfer in a DeLaval Nozzle", Ph.D. Thesis, Chemical Engineering, Purdue University, Aug. 1957.

18. Robison, D. E., "Experimental Performance and Heat Transfer of a Rocket Motor Operating on WFNA-JF-3 at 700 psia Chamber Pressure and 500 lb Thrust", MS Thesis, Mechanical Engineering, Purdue University, June 1952.

19. Saunders, O. A. and Calder, P. H., "Some Experiments on the Heat Transfer from a Gas Flowing Through a Convergent-Divergent Nozzle", Heat Transfer and Fluid Mechanics Institute, Preprints of papers presented at Stanford University, June 1951.

20. Schlichting, Hermann, Boundary Layer Theory, McGraw-Hill, 1955.

21. Sibulkin, M. "Heat Transfer to an Incompressible Turbulent Boundary Layer and Estimation of Heat Transfer Coefficients at Supersonic Nozzle Throats", Journal of the Aeronautical Sciences, Feb. 1956.

22. Sibulkin, M. "Boundary-Layer Measurements at Supersonic Nozzle Throats", Report No. 20-97, Jet Propulsion Laboratory, California Institute of Technology, 1952.

23. United States Steel Co. "Fabrication of U.S.S. Stainless and Heat Resisting Steels" United States Steel, Pittsburgh, Pa., 1952.

24. Warner, C. F. and Zucrow, M. J., "An Evaluation of Heat Transfer Encountered in a Rocket Motor Operating at High Chamber Pressures", Project Squid Technical Report No. 18, Purdue University, July 1949.

BIBLIOGRAPHY (Continued)

25. Wolf, H., "The Experimental and Analytical Determination of the Heat Transfer Characteristics of Air and Carbon Dioxide in the Thermal Entrance Region of a Smooth Tube with Large Temperature Differences Between the Gas and Tube Wall", Ph.D. Thesis, Mechanical Engineering, Purdue University, Jan. 1958.

26. Zucrow, M. J., Jet Propulsion and Gas Turbines, John Wiley and Sons, Inc., 1948.

27. Rose, R. K., "Experimental Determination of the Heat Flux Distribution in a Rocket Nozzle, MSME Thesis, Purdue University, January 1958.